Materials Today Bio 31 (2025) 101555

Contents lists available at ScienceDirect

Materials Today Bio

journal homepage: www.journals.elsevier.com/materials-today-bio

Enzyme-responsive vitamin D-based micelles for paclitaxel-controlled delivery and synergistic pancreatic cancer therapy

Diana Peixoto [a,b,c], João M. Ravasco [d,e], Barbara Blanco-Fernandez [c], Francisco Veiga [a,b], Angel Concheiro [c], João Conde [d,e,**], Ana Cláudia Paiva-Santos [a,b,***], Carmen Alvarez-Lorenzo [c,*]

[a] Department of Pharmaceutical Technology, Faculty of Pharmacy of the University of Coimbra, University of Coimbra, 3000-548 Coimbra, Portugal
[b] REQUIMTE/LAQV, Group of Pharmaceutical Technology, Faculty of Pharmacy of the University of Coimbra, University of Coimbra, 3000-548 Coimbra, Portugal
[c] Departamento de Farmacología, Farmacia y Tecnología Farmacéutica, I+D Farma (GI-1645), Faculty of Pharmacy, iMATUS and Health Research Institute of Santiago de Compostela (IDIS), University of Santiago de Compostela, 15782, Santiago, Spain
[d] Comprehensive Health Research Centre, NOVA Medical School, Faculdade de Ciências Médicas, NMS, FCM, Universidade Nova de Lisboa, 1169, Lisboa, Portugal
[e] Research Institute for Medicines (iMed.ULisboa), Faculty of Pharmacy, University of Lisbon, 1649, Lisbon, Portugal

ARTICLE INFO

Keywords:
Pancreatic ductal adenocarcinoma
Bioactive vitamin D_3 conjugate
Esterase-activatable micelle
Intracellular drug delivery
Paclitaxel

ABSTRACT

Pancreatic ductal adenocarcinoma (PDAC) remains one of the most feared diseases worldwide owing to its poor prognosis, negligible therapeutic advances, and high mortality. Herein, multifunctional enzyme-responsive micelles for the controlled delivery of paclitaxel (PTX) were prepared to circumvent its current clinical challenges. Accordingly, two enzyme-responsive structural units composed of Vitamin D_3 (VD_3) conjugated with polyethylene glycol of different molecular weights (600 Da and 2000 Da) were synthesized and characterized using different analytical methods. By applying the solvent evaporation method, these bioactive structural units self-assembled into sub-100 nm VD_3 micelles with minimal batch-to-batch variation, monomodal particle size distribution, and high encapsulation efficiency. The enzyme-triggered disassembly of PTX-loaded VD_3 micelles was demonstrated by release studies in the presence of a high esterase content typically featured by PDAC cells. PTX-loaded VD_3 micelles also exhibited prominent cell internalization and induced a considerable cytotoxic synergistic effect against human PDAC cells (BxPC-3 cells) in 2D and 3D cell culture models compared with free PTX. The PTX-loaded VD_3 micelles were hemocompatible and stable after long-term storage in the presence of biorelevant media, and showed higher efficiency to inhibit the tumor growth compared to the approved clinical nanoformulation (Abraxane®) in an *in ovo* tumor model. The findings reported here indicate that VD_3S-PEG micelles may have a promising role in PDAC therapy, since VD_3 could act not only as a hydrophobic core of the micelles but also as a therapeutic agent that provides synergetic therapeutic effects with the encapsulated PTX.

1. Introduction

Pancreatic ductal adenocarcinoma (PDAC) is a highly aggressive and lethal disease worldwide, with only approximately 12 % of patients alive 5 years after diagnosis [1,2]. Typically, patients with PDAC often present with locally advanced or metastatic stages (approximately 80 % of cases) owing to the rapid progression, highly invasive and immunosuppressive tumor microenvironment (TME), lack of specific clinical manifestations, and late diagnosis [3,4]. In advanced or metastatic PDAC, modest response rates are obtained using multi-agent chemotherapy regimens, such as FOLFIRINOX (i.e., a four-drug combination consisting of 5-fluorouracil, irinotecan, oxaliplatin, and leucovorin) or gemcitabine (GEM) in combination with nanoparticle albumin-bound (nab) paclitaxel (nab-PTX, Abraxane®) [5], providing

* Corresponding author. Departamento de Farmacología, Farmacia y Tecnología Farmacéutica, Faculty of Pharmacy, iMATUS and Health Research Institute of Santiago de Compostela (IDIS), University of Santiago de Compostela, 15782, Santiago de Compostela, Spain.
** Corresponding author. Comprehensive Health Research Centre, NOVA Medical School, Faculdade de Ciências Médicas, NMS, FCM, Universidade Nova de Lisboa, 1169, Lisboa, Portugal.
*** Corresponding author. Department of Pharmaceutical Technology, Faculty of Pharmacy of the University of Coimbra, University of Coimbra, 3000-548 Coimbra, Portugal.
E-mail addresses: joao.conde@nms.unl.pt (J. Conde), acsantos@ff.uc.pt (A.C. Paiva-Santos).

https://doi.org/10.1016/j.mtbio.2025.101555
Received 16 September 2024; Received in revised form 20 December 2024; Accepted 3 February 2025
Available online 4 February 2025
2590-0064/© 2025 The Authors. Published by Elsevier Ltd. This is an open access article under the CC BY-NC license (http://creativecommons.org/licenses/by-nc/4.0/).

a median overall survival of only 11.1 [6] and 8.5 months [7], respectively. Apart from their short-term benefits and limited patient survival, these treatments are associated with systemic toxicity, rapid blood clearance, and the emergence of multiple drug resistance (MDR) [3,8].

PTX is a well-known and potent chemotherapeutic agent included in the list of essential medicines of the World Health Organization (WHO) because of its application in several types of cancers [9]. PTX is a diterpenoid centered around a bulky taxane ring with several hydrophobic substituents classified as biopharmaceutical classification system (BCS) class IV drugs (i.e., low solubility and low permeability). Consequently, the therapeutic potential of PTX in PDAC treatment is challenged by its unfavorable physicochemical properties, including high molecular weight (853.91 g/mol), lipophilicity (logP around 3.66 and water solubility <0.30 μg/mL), and recrystallization upon dilution [10]. In addition, the efficacy of PTX is seriously affected by its short half-life (*ca.* 6 h) and the emergence of MDR [9,11]. Therefore, the first intravenous formulation of PTX (Taxol®), approved in 1993 by the Food and Drug Administration (FDA), required the nonionic surfactant Cremophor® polyoxyethylated castor oil (EL) in dehydrated ethanol (1:1, v/v) as a vehicle to improve the solubility of PTX. However, Cremophor® EL is not well tolerated (dose-limiting toxicity) and PTX formulated with CrEL can induce severe clinical acute hypersensitivity reactions. As an alternative, nab-PTX consisting of human serum albumin-PTX nanoparticles (*ca.* 130 nm particle size) was developed to address the dose-limiting toxicity of Cremophor® EL due to its capacity to dissociate into soluble albumin-bound PTX complexes after intravenous administration [12,13]. Since 2013, Abraxane® combined with GEM has been a treatment option for patients with advanced-stage metastatic PDAC [14]. Although this combination therapy minimizes hypersensitivity reactions and slightly enhances the median overall survival compared to free GEM (8.5 and 6.6 months, respectively), an increased incidence of hematologic toxicity and sensory neuropathy has also been reported [13]. In nab-PTX, human serum albumin was included as a natural solubilizer of PTX, but not as a tumor-targeting carrier or as a bioactive excipient. Therefore, this formulation rapidly dissociates after intravenous administration, resulting in nonspecific free PTX distribution through the organism [15,16]. The search for improved safety and therapeutic efficacy of PTX has been reflected in the recent approval of various parenteral PTX-loaded nanoformulations for the treatment of different types of cancer, including polymeric micelles (Genexol-PM®, South Korea, and Nanoxel®, India), liposomes (Lipusu®, China), and polymer-drug conjugates (Opaxio™, USA) [17]. In addition, a lipid-based oral formulation of PTX (Liporaxel®, South Korea) has been approved for gastric cancer treatment [18]. Nevertheless, none of these formulations has been translated into clinical PDAC therapies.

Micelles are being widely studied in preclinical and clinical trials as versatile long-circulating delivery systems for highly hydrophobic chemotherapeutic agents, which are either covalently attached to polymer chains or non-covalently encapsulated in micelles [17–19]. The encapsulation of chemotherapeutic agents into the hydrophobic core of micelles improves their overall pharmacokinetic profile, since micelles increase drug solubilization, provide protection against enzymatic degradation, present tunable physicochemical characteristics, and are able to release their payload in a controlled manner over time [21]. The hydrophilic outer shell of micelles provide "stealthness" and circumvent recognition and elimination by the reticuloendothelial system (RES) [20,21], facilitating prolonged blood circulation time with preferential accumulation in tumors having leaky vasculatures and impaired lymphatic drainage (enhanced permeability and retention (EPR) effect). The unique TME of PDAC allows the design of site-specific stimuli-responsive micelles that can efficiently deliver drugs to the tumor site [24]. Lower pH of the tumor core (pH~6.5 *vs.* external stroma pH~7.4) [25] and the excessive enzyme secretion of PDAC TME compared to healthy tissues (i.e., matrix metalloproteinases, hyaluronidase, β-glucuronidase, and esterases) can serve as internal stimuli. For example, linkers activated by esterases (e.g., ester bond linkers) have been incorporated into the structural units of micelles to trigger drug release *via* intracellular catalytic esterases [26].

Vitamin D (VD) is a hydrophobic secosteroid prohormone that has received increasing attention in cancer development and prognosis [27]. Although the main forms of VD consist of cholecalciferol (VD_3) and ergocalciferol (VD_2), the physiological role of VD is primarily mediated by its metabolite calcitriol, which binds to a specific high-affinity receptor, the VD Receptor (VDR) [28,29]. In particular, calcitriol may play a role in regulating several signaling pathways involved in cellular proliferation, cell cycle regulation, apoptosis, angiogenesis, inflammation, invasion, and metastasis [26,27]. Furthermore, calcitriol has also been shown to circumvent MDR [30] by inhibiting P-glycoprotein (P-gp) [31] and multidrug resistance-associated protein 1 (MRP1) [32] in several types of cancer cells expressing VDR, including PDAC cells [25,27]. In addition, the synergistic effects of calcitriol when concomitantly administered with conventional chemotherapy have been reported for PDAC [31,32]. VD also exhibits antifibrotic activity towards the desmoplastic stroma of PDAC, which acts as a mechanical barrier around cancer cells, preventing proper vascularization and, thus, limiting exposure to chemotherapy [35,36]. Upon activation of VDR in cancer-associated fibroblasts (CAFs), VD can reprogram the pro-desmoplastic and pro-tumorigenic features to a quiescent phenotype without ablating the stroma architecture, resulting in fibrosis reduction and improved chemotherapy outcomes in preclinical studies [33,34]. Several clinical studies combining VD with different chemotherapeutic agents are currently ongoing, including patients with previously untreated metastatic PDAC (ClinicalTrials.gov identifier NCT02030860) [4,5]. VD also has immunomodulatory, anti-inflammatory, and antioxidant properties [37]. Collectively, these properties have prompted the design of VD-based derivatives to provide controlled release of chemotherapeutic agents, improve their tumor bioavailability, and achieve synergistic therapeutic effects [38]. For instance, VD_3 glutarate-PEG [39] and VD_3-hyaluronic acid conjugates [40] have been explored as structural units of micelles to encapsulate doxorubicin for breast cancer treatment. Additionally, VD_3-drug conjugates (prodrugs) can self-assemble into biocompatible, biodegradable, and non-toxic nanoplatforms for the successful delivery of chemotherapeutic drugs such as PTX [41], doxorubicin [42], and cisplatin [42]. However, VD_3-based nanoplatforms are still underexploited for drug delivery in advanced and metastatic PDAC therapies.

The present study aimed to develop enzyme-responsive VD_3-based micelles for the intravenous or intratumoral delivery of PTX, with a sub-100 nm particle size than can facilitate access to tumor cells and avoid premature elimination in the kidney (<6 nm), liver (>150), and spleen (>200 nm). Accordingly, VD_3 succinate (VD_3S)-PEG conjugates were synthesized as water-soluble derivates of VD_3 composed of a hydrophilic polar (water-soluble) head and a lipophilic (water-insoluble) alkyl tail connected by an enzyme-cleavable ester bond. Two terminally methylated PEGs with different chain lengths, 600 Da and 2000 Da, were selected to chemically synthesize the VD_3S-PEG_{600} and VD_3S-PEG_{2000} conjugates in a short two-step synthesis. The effect of PEG chain length on the ability of the developed VD_3S-PEG conjugates to self-assemble into mono-dispersed nano-sized core-shell micellar structures was assessed. Blank and PTX-loaded micelles (PTX+VD_3S-PEG micelles) using both types of VD_3S-PEG conjugates were produced using the solvent evaporation method and characterized in terms of particle size, polydispersity index (PDI), zeta potential (ZP), morphology, and encapsulation efficiency. Then, the release profile, enzyme responsiveness, and serum stability of the micelles were investigated. After structural characterization, the hemocompatibility, cellular uptake, and anticancer activity of the PTX+VD_3S-PEG micelles were evaluated. According to the FDA Modernization Act 2.0 [43], more human-relevant testing methods are needed to replace animal experiments, due to the poor correlations found in some diseases between the outcomes in different species. This is particularly relevant in the case of PDAC since preclinical models can hardly replicate the disease in humans [44].

Thus, pre-screening of the formulations was carried out using both two-dimensional (2D) and three-dimensional (3D) models based on human PDAC cells (BxPC-3). Considering the 3R guiding principle (i.e., reduction, refinement, and replacement of animal models) highly supported by the European Parliament Directive 2010/63/EU and the recent FDA Modernization Act 3.0 [45], the *in ovo* chorioallantoic membrane (CAM) assay was performed as an alternative *in vivo* model for the evaluation of the antitumor activity of PTX+VD_3S-PEG micelles.

2. Materials and methods

2.1. Materials

PTX ($C_{47}H_{51}NO_{14}$, M_W 853.9 g/mol) and VD_3 ($C_{27}H_{44}O$, M_w 384.64 g/mol) were supplied by Thermo Scientific Alfa Aesar (Karlsruhe, Germany). PEG ($C_6H_{14}O_4$, M_w 2000 g/mol) was from CymitQuímica, S.L. (Barcelona, Spain). PEG ($C_6H_{14}O_4$, M_w 600 g/mol) was obtained from CARLO ERBA Reagents (Milan, Italy). Abraxane® (Bristol Myers Squibb) was acquired through the Clinic University Hospital (Santiago de Compostela, Spain). Ethanol absolute 99.9 % (EtOH) and acetonitrile HPLC LC-MS grade (CH_3CN) were purchased from VWR chemicals (Fontenary-Sous-Bois, France). 4-(Dimethylamino)pyridine (DMAP), dry dichloromethane (DCM), chloroform, magnesium sulfate ($MgSO_4$), diethyl ether, the pyrene fluorescence probe, polysorbate 80, sodium sulfite (Na_2SO_3), Triton™ X-100, and porcine liver esterase (PLE) were acquired from Sigma Aldrich (St. Louis, MO, SA). Sulfuric acid (H_2SO_4) was purchased from Merck Millipore (Darmstadt, Germany). N-(3-dimethyl aminopropyl)-N′-ethyl carbodiimide hydrochloride (EDC), formamide, and α-bromonaphthalene were purchased from Fischer Scientific (Lough-borough, UK). Nile Red was purchased from Invitrogen (Eugene, OR, USA). All solvents employed were of HPLC or synthesis grade. Ultrapure water (resistivity>18.2 MW cm; Milli-Q®, Millipore Ibérica, Madrid, Spain) was obtained using reverse osmosis. Phosphate-buffered saline (PBS) solution (pH7.4) was prepared according to the European Pharmacopoeia 6th edition.

2.2. Synthesis of cholecalciferol succinate

In a pressure tube, cholecalciferol (500 mg, 1.3 mmol, 1 equiv, Figs. S1 and S10) was dissolved in chloroform (7 mL) under a nitrogen atmosphere. Succinic anhydride (1.56 g, 15.6 mmol, 12 equiv) was added, followed by DMAP (34.9 mg, 0.3 mmol, 0.22 equiv). The reaction mixture was stirred for 16h at 80 °C and protected from light. The reaction was monitored by thin layer chromatography (TLC). The reaction mixture was filtered, diluted in cold chloroform, and washed with 1M HCl (2 × 10 mL) and brine (3 × 10 mL). The organic phase was dried using anhydrous $MgSO_4$ and the organic phase was evaporated under vacuum and the solid washed with cold diethyl ether to afford pure cholecalciferol succinate (VD_3S, Figs. S2 and S11) as a white solid (598 mg, 95 % yield).

2.3. Synthesis of cholecalciferol succinate-polyethylene glycol conjugate

In a round-bottom flask, VD_3S (250 mg, 0.51 mmol, 1 equiv) was dissolved in dry DCM (5 mL) under nitrogen atmosphere. EDC.HCl (118.7 mg, 0.62 mmol, 1.2 equiv) was added, followed by PEG of 600 Da (0.62 mmol, 1.2 equiv, Figs. S3 and S12) or 2000 Da (0.62 mmol, 1.2 equiv, Figs. S4 and S13) and DMAP (12.6 mg, 0.1 mmol, 0.2 equiv). The reaction mixture was stirred overnight and protected from light. Past this time, the reaction was filtered, diluted in cold chloroform, and washed with 1M HCl (2 x 10 mL), and brine (3x 10 mL). The organic phase was dried using anhydrous $MgSO_4$ and the organic phase was evaporated under vacuum and the solid washed with cold diethyl ether to afford pure VD_3S-PEG_{600} (555 mg, 62.3 % yield, Figs. S5 and S14) or VD_3S-PEG_{2000} (1.3 g, 78 % yield, Figs. S6 and S15).

2.4. Characterization of cholecalciferol glutarate-polyethylene glycol conjugate

All synthetic compounds were characterized using Fourier transform infrared (FT-IR) spectroscopy and nuclear magnetic resonance spectroscopy (^{1}H and ^{13}C NMR). NMR spectra of pure compounds (i.e., VD_3, PEG_{600}, and PEG_{2000}), VD_3S and VD3S-PEG conjugates were recorded in a Bruker Fourier 300 spectrometer (300 MHz for ^{1}H and 75 MHz for ^{13}C). Chemical shifts were expressed in parts per million (ppm, δ scale) referenced to tetramethylsilane as internal standard with δ 7.26 ppm (^{1}H in $CDCl_3$) and δ 77.16 ppm (^{13}C in $CDCl_3$). The multiplicity of the signals was reported as s (singlet), d (doublet), t (triplet), and m (multiplet). All coupling constants (J) were given in hertz (Hz). FTIR spectra were recorded between 4000 cm^{-1} and 400 cm^{-1} at room temperature (RT) using a FT-IR spectrometer Alpha II (Bruker Optic GmbH, Ettlingen, Germany). Spectra analysis was conducted using the MestreNova® v14.0 software (Mestrelab® Research Inc., Spain), as described in the Supplementary Material (Figs. S1–S15).

2.5. Contact angle of cholecalciferol succinate-polyethylene glycol conjugate

VD_3S-PEG_{600} conjugate was placed on glass slides and dried. The contact angle was recorded, in triplicate at RT, immediately after dropping (*ca.* 5 μL) an apolar liquid (i.e., α-bromonaphthalene) and two polar liquids (i.e., water and formamide) using a Phoenix-300 plus video-based optical goniometer (SEO, Korea) fitted with a video camera that allowed for image acquisition and data analysis. The degree of hydrophobicity of the VD_3S-PEG_{600} conjugate was evaluated using the method of Good and Van Oss [46], as described in the Supplementary Material.

2.6. Determination of critical micelle concentration

The critical micellar concentration (CMC) of the VD_3S-PEG_{600} micelles was determined using the fluorescence probe method. Briefly, solutions (1 mL) containing VD_3S-PEG_{600} conjugate at various concentrations (0.05, 0.1, 0.5, 1, 5, 10, 50, 100, 500, 1000, and 5000 μg/mL) in PBS were poured into vials, to which aliquots (20 μL) of pyrene solution (0.15 mM) in EtOH were added (final concentration 3 μM) [47]. The resulting solutions were equilibrated at RT and protected from light for 2 h under magnetic stirring (200 rpm). Subsequently, the organic solvent was left to evaporate overnight at RT [48]. Pyrene fluorescence emission spectrum was recorded on a Jasco FP-8350 UV–Vis spectrofluorometer at 25 ± 2 °C from 340 to 450 nm using an excitation wavelength of 335 nm. The ratio of the first (I_1) to third (I_3) excitation peak was used as an indicator of micelle formation. I_1/I_3 indicates the polarity of the medium in which pyrene is dissolved, and the CMC values can be assessed from the inflection point in the plot of I_1/I_3 versus concentration [49,50].

2.7. Preparation of paclitaxel-loaded micelles

PTX-loaded micelles composed of either VD_3S-PEG_{600} or VD_3S-PEG_{2000} were prepared using the solvent evaporation method [48,51]. VD_3-PEG conjugates and PTX were dissolved in EtOH (1 mL) using different VD_3S-PEG conjugate/drug mass ratios (i.e., 25:5, 25:1.2, 25:1, and 50:1 w/w). Subsequently, the suspension was stirred (200 rpm) at RT until PTX was completely dissolved, and the flasks were covered to avoid EtOH evaporation. The dispersion was then added dropwise to a PBS solution (1 mL, pH~7.4) with constant stirring (200 rpm) either manually (1 drop/5s) [10] or using a volumetric dispenser (0.15 mL/min, programmable single-channel infusion syringe pump, World Precision Instruments, Sarasota, Florida, USA) [49]. The formulations were stirred (200 rpm) for 2 h and the organic solvent was left to evaporate overnight (14–16 h) at RT. The excess non-incorporated PTX

and VD_3S-PEG conjugate aggregates were removed by filtration (0.22 μm PTFE hydrophilic syringe filters) before characterization [48]. Filtration was applied to provide sterility to the samples in a single step when necessary. Blank micelles were prepared following the same protocol but without the addition of PTX (Fig. S22). Compositions of the prepared micellar formulations and dropwise addition methods are listed in Table 1. The micellar formulations were designated with **B** and **F** codes, followed by a number referring to blank micelles **(B)** and paclitaxel-loaded micelles **(F)**. All micellar formulations were freshly prepared prior to each experiment. In circumstances where micelles needed to be stored for further use, they were kept at 4 ± 2 °C.

2.8. Characterization of paclitaxel-loaded micelles

The mean particle size, PDI, and ZP of the blank and PTX-loaded micellar dispersions were determined by dynamic light scattering (DLS) and electrophoretic light scattering (ELS) in folded capillary cuvettes (DTS1070) using a Zetasizer® Pro-Blue (Malvern Instruments, UK) with a fixed detection angle of 173° (non-invasive backscatter), a refractive index of 1.33, and automatic attenuation at 25 °C. The micellar dispersions were directly measured without dilution. The results quoted are the averages of triplicate measurements based on the intensity and number of four different batches of micelles, with at least 8 readings of particle size and ZP of micellar dispersions in PBS pH 7.4. The pH was measured with a calibrated HI981032 pH Tester (Hanna Instruments, USA) at RT, without any previous dilution. The morphology of the blank micelles (25 mg/mL) was characterized by 2 % phosphotungstic acid staining using a JEOL JEM1011 transmission electron microscope (TEM) operating at 80 kV. The particle size of the micelles was manually determined by counting more than 100 particles in the TEM micrographs.

2.9. Drug loading and encapsulation efficiency

PTX from VD_3S-PEG micelles was identified and quantified by High-Performance Liquid Chromatography (HPLC) with ultraviolet (UV) detection following a previously developed method [49], as described in detail in the Supplementary Material (Figs. S17–S19, Table S3). The concentration of PTX was quantified using a JASCO (Tokyo, Japan) HPLC (AS-4140 Autosampler, PU-4180 Pump, LC-NetII/ADC Interface Box, CO-4060 Column Oven, MD-4010 Photodiode Array Detector), fitted with a C18 column (Waters Symmetry C18, 5 μm, 4.6 × 250 mm), and operated with ChromNAV software (JASCO, Tokyo, Japan). To validate the method for the identification and quantification of PTX, a stock solution of PTX (100 μg/mL) was freshly prepared in acetonitrile. This stock solution was used to prepare 10 calibration standard solutions on the day of analysis, presenting concentrations ranging from 0.25 μg/mL to 50 μg/mL. The calibration standard solutions were filtered through PTFE hydrophilic syringe filters (diameter, 13 mm; pore size 0.22 μm from Scharlab-Scharlau, Barcelona, Spain), transferred to HPLC vials, and analyzed using the proposed analytical method by injecting each concentration (Table S3). The method was validated according to the International Council for Harmonisation of Technical Requirements for Pharmaceuticals for Human Use (ICH) and the Food and Drug Administration (FDA) guidelines, considering the system suitability, linearity (correlation coefficient, $r^2 > 0.9998$), accuracy (coefficient of variation of the response factors <2 %), and precision (coefficient of variation of repeated measurements <2 %). The lowest concentration at which PTX could be detected or quantified with good accuracy and precision was determined according to the standard deviation of the response and the slope of the linear regression of the calibration curve ($y = 111281x+221.68$, Fig. S20). The estimated limits of detection (LOD) and quantification (LOQ) were 0.288 and 0.873 μg/mL, respectively. The recovery percentage was 99.53 %, ensuring data quality during HPLC analysis.

To quantify the drug-loading content (DL) and encapsulation efficiency (EE), the PTX-loaded micellar solution (200 μL) was collected, diluted (1:50) with acetonitrile, and vortexed to disrupt the self-assembled structure and extract the encapsulated PTX. The collected sample was filtered through 0.22 μm PTFE hydrophilic syringe filters, and the PTX concentration was determined by HPLC, as explained above. DL and EE were calculated as follows [51,53]:

$$\text{D.L. } (\%) = \frac{\text{Mass of PTX in micellar solution}}{\text{Mass of VD}_3\text{S-PEG conjugate} + \text{Initial mass of PTX}} \times 100\ \% \quad (1)$$

$$\text{E.E. } (\%) = \frac{\text{Mass of PTX in micellar solution}}{\text{Initial mass of PTX in micellar solution}} \times 100\ \% \quad (2)$$

2.10. Stability of paclitaxel-loaded micelles

The long-storage stability of PTX-loaded and blank micelles in PBS (pH~7.4) was assessed by monitoring the particle size, and PDI at different temperatures (i.e., 4 ± 2 °C, 25 ± 2 °C, and 37 ± 2 °C) over a period of 4 weeks. All micellar formulations were protected from light to prevent VD_3 and PTX degradation. Next, the colloidal stability of PTX+VD_3S-PEG micelles was assessed in RPMI-1640 cell culture media supplemented with 10 % fetal bovine serum, 1 % penicillin/streptomycin (1:1 v/v), fetal bovine serum (FBS) (1:1 v/v), and human blood plasma (1:1 v/v) to mimic the physiological environment after intravenous administration [54]. The samples were kept under gentle agitation (100 rpm) in an orbital incubator at 37 °C to simulate the physiological conditions. Particle size and PDI variations of the

Table 1
Components used to prepare the blank **(B)** and PTX-loaded **(F)** micelles.

Formulation code	VD_3-PEG_{2000} (mg)	VD_3S-PEG_{600} (mg)	PTX (mg)	EtOH (mL)	PBS (mL)	Dropwise method	VD_3S-PEG/PTX ratio (w/w)
B_1	25	–	–	1	1	1 drop/5s[a]	–
B_2	–	25	–	1	1	1 drop/5s[a]	–
B_3	25	–	–	1	1	0.15 mL/min[b]	–
B_4	–	25	–	1	1	0.15 mL/min[b]	–
B_5	50	–	–	1	1	0.15 mL/min[b]	–
B_6	–	50	–	1	1	0.15 mL/min[b]	–
F_1	25	–	5	1	1	1 drop/5s[a]	25:5
F_2	–	25	5	1	1	1 drop/5s[a]	25:5
F_3	25	–	1.2	1	1	0.15 mL/min[b]	25:1.2
F_4	–	25	1.2	1	1	0.15 mL/min[b]	25:1.2
F_5	25	–	1	1	1	0.15 mL/min[b]	25:1
F_6	–	25	1	1	1	0.15 mL/min[b]	25:1
F_7	50	–	1	1	1	0.15 mL/min[b]	50:1
F_8	–	50	1	1	1	0.15 mL/min[b]	50:1

[a] Dispersion containing VD_3S-PEG conjugate and PTX was slowly added dropwise *via a* syringe with constant magnetic stirring (ca 1 drop/5s).
[b] Dispersion containing VD_3S-PEG conjugate and PTX was added dropwise *via* an infusion/syringe pump with constant magnetic stirring (0.15 mL/min).

PTX+VD_3S-PEG micelles were monitored at different time points for 24 h. All measurements were performed in triplicate, and the results are reported as mean ± standard deviation.

2.11. In vitro paclitaxel release kinetics

PTX release kinetics from the VD_3S-PEG_{600} and VD_3S-PEG_{2000} micelles were evaluated using the dialysis method at 37 °C and different pH values, mimicking the PDAC TME (pH~6.5) and normal physiological conditions (pH~7.4) [25]. A small volume of HCl 1M was used to adjust the pH of the release medium. Prior to use, activation of the dialysis membrane (molecular cut-off of 12,400 Da; Sigma-Aldrich, Spain) was performed as indicated by the manufacturer. Freshly prepared PTX+VD_3S-PEG micelles (1 mL) were placed into dialysis membrane bags, sealed, and immersed in the release medium (12 mL of PBS pH~7.4 or pH~6.5, containing 0.5 % (w/v) polysorbate 80). The release experiment was conducted in an orbital incubator shaker set at 100 rpm, with a fixed incubation temperature of 37 °C in the dark. At predetermined time points, aliquots of the release medium (1 mL) were withdrawn to determine PTX release and immediately replaced with an equal volume of fresh release medium to maintain sink conditions [23]. PTX concentration was monitored at 227 nm using HPLC, as previously described. Assays were performed in quadruplicate, and the results are reported as mean ± standard deviation.

2.12. Enzyme responsiveness of paclitaxel-loaded micelles

The enzymatic sensitivity of PTX+VD_3S-PEG_{600} micelles to enzymatic hydrolysis was determined in the presence of porcine liver esterase (PLE). Freshly prepared PTX+VD_3S-PEG micelles (1 mL) were diluted in PBS (pH~6.5 or pH~7.4) in the presence of PLE (500 μL of PLE prepared in PBS (pH~6.5 or pH~7.4), to obtain a final concentration of 50 U/mL) and incubated for 24 h at 37 °C under gentle agitation. Alterations in the particle size and PDI of PTX+VD_3S-PEG micelles were monitored by DLS, and the morphology of the micelles was evaluated by TEM. The release of PTX and VD_3 from VD_3S-PEG_{600} micelles was investigated at 37 °C under gentle agitation (100 rpm) with PBS (pH 6.5 or pH 7.4), containing 0.5 % polysorbate 80 (w/v) in the presence or absence of 50 U/mL esterase as release media. PTX+VD_3S-PEG_{600} micelles dispersed in release media (1 mL) were quickly sealed into a dialysis membrane tube (molecular cut-off of 12,400 Da; Sigma-Aldrich, Spain) and instantly immersed in prewarmed release media (12 mL). Aliquots of the release medium were collected (1 mL) at predesigned time points and replaced with fresh release media (1 mL) to keep the volume of the entire release system constant. The collected samples were dissolved in acetonitrile for HPLC analysis. A specific HPLC-UV method, described in detail in the Supplementary Material (Figs. S27–S29, Table S6), was developed to identify and quantify the VD_3 released from VD_3S-PEG_{600} micelles.

2.13. Human cell line and culture conditions

Human pancreatic cancer BxPC-3 cells (ATCC CRL-1687™, USA) with epithelial-like morphology were kindly supplied by the Translational Medical Oncology (Oncomet), Health Research Institute of Santiago (IDIS), University Hospital of Santiago (SERGAS). BxPC-3 cells were cultured using RPMI-1640 medium (Gibco™ RPMI 1640 Medium, GlutaMAX™ Supplement) supplemented with 10 % fetal bovine serum (FBS, Gibco™) and 1 % antibiotic (streptomycin and penicillin) solution (Sigma Aldrich, St. Louis, MO, USA) in T-75 culture flasks (Fisher Scientific) at 37 °C in a humidified atmosphere containing 5 % CO_2. After approximately 80 % confluence was reached (80 % of the surface of the cell culture dish was covered by a cell monolayer), cells were routinely trypsinized and sub-cultured using a 1:3 split ratio. Visual estimation of the cells covering approximately 80 % of the flask was sufficiently precise. Typically, it takes approximately 48 h to reach 80 % confluence, depending on the growth rate and seeding density of the cells.

2.14. Assessment of cellular uptake by confocal microscopy

Internalization of PTX+VD_3S-PEG_{600} micelles by BxPC-3 cells was analyzed by confocal laser scanning microscopy (CLSM), using Nile Red (NR) as a hydrophobic fluorescence probe (Ex/Em 552/636 nm). PTX+VD_3S-PEG_{600} micelles were prepared as previously described for PTX+VD_3S-PEG micelles **(Section 2.7)**. The hydrophobic chromophore, NR (0.05 mg), was dissolved in EtOH (1 mL) and stirred for 1 h at RT. Then, 0.1 mL of NR (50 μg/mL in EtOH) was mixed with the VD_3S-PEG_{600} conjugate (50 mg/mL) before addition to the aqueous phase and evaporation of the organic solvent (final NR concentration of 0.5 μg/mL). The dispersion was added dropwise to 1X PBS (1 mL, pH~7.4) and stirred (200 rpm) for 2 h at RT. The reaction mixture was left to evaporate overnight at RT to remove the EtOH. Unloaded NR precipitated in the aqueous phase was removed by filtration (0.22 μm PTFE hydrophilic syringe filters). Subsequently, a reddish color was obtained. BxPC-3 cells were cultured according to a previously described method **(Section 2.13.)** and seeded in 8-well glass plates (0.7 cm^2, Lab-Tek™ II Chamber Slide System, Thermo Scientific™ Nunc™, Waltham, MA, USA) at a cell seeding density of 10,000 cells/well. After 24 h of incubation (37 °C, 5 % CO_2 and 90 % RH), the cell culture medium was removed and replaced by the NR-loaded micellar solution in cell culture medium (equivalent concentration of PTX was 10 μM). Subsequently, the cells were incubated with the NR-loaded micelles for 1 h, 4 h, and 24 h at 37 °C. At these time points, the micellar solution was carefully removed, and the cells were rinsed three times with ice-cold 1X PBS (pH~7.4). Then, cells were fixed with a 4 % (w/v) paraformaldehyde solution in 1X PBS (pH~7.4) (100 mL/well) for 10 min at RT and rinsed three more times with PBS. After fixation, the cells were permeabilized with Triton X-100™ (0.05 % (w/v) in PBS) for 5 min at RT and washed again with 1X PBS (pH~7.4) three times. Afterwards, the cell cytoskeleton (filamentous actin) was stained with Alexa Fluor 488 phalloidin (Invitrogen™, Ex/Em 490/525 nm, 1:300 in 1X PBS, 45 min, RT) in the dark. After three washing steps with 1X PBS the cell nuclei were stained with 4′,6-diamidino-2-phenylindole (DAPI, Ex/Em 340/488 nm, Sigma Aldrich, 1:1000 in 1X PBS, 10 min, RT) in the dark before mounting using ProLong Diamond Antifade mounting media (Thermo Fischer Scientific, USA) and a rectangular cover slip (24 × 60 mm, VWR®, Darmstadt, Germany). The slides were cured for 48 h at 4 °C in the dark. Experiments were performed in triplicate, and positive (free NR, 0.5 μg/mL) and negative (RPMI cell culture medium) controls were included to identify possible artifacts of exposure methodology and guarantee the reliability of the assay. Fixed cells were imaged using a Confocal Laser Scanning Microscope Stellaris 8 FALCON (Leica Microsystems, Wetzlar, Germany) equipped with a CS2 Plan Apochromat 93x/NA 1.3 glycerol immersion objective lens, a 405 nm diode, and White Light Lasers (WLL) for excitation. Images (xyz) were collected using a sequential acquisition mode with lightning adaptive deconvolution (Leica Microsystems, Wetzlar, Germany), an optimized xy projection, and a z-axis sectioning interval of 0.3 μm. The green channel was used for phalloidin (λexc = 499 nm, λem = 505–550 nm), the red channel for Nile Red-loaded micelles (λexc = 530 nm, λem = 590–650 nm), and the blue channel for DAPI (λexc = 405 nm, λem = 410–480 nm). Image analysis was performed using the Leica SP8 LAS X Life Science Microscope Software (Version 3.5.5, Leica, Germany).

2.15. In vitro cytotoxicity of paclitaxel-loaded micelles in 2D cell culture models

The cytotoxicity of free PTX, free VD_3, blank VD_3S-PEG_{600} micelles, PTX+VD_3S-PEG_{600} micelles, and the clinically approved nanoparticle formulation Abraxane® in 2D PDAC culture models was evaluated using the Alamar Blue assay (resazurin cell viability assay) [55]. Briefly, BxPC-3 cells were seeded in 96 well bottom plates (Corning, USA) at a

density of 10, 000 cells/well in RPMI complete medium for 24 h. Then, each test formulation at various concentrations of PTX or equivalent (0.0001, 0.001, 0.01, 1, 10, and 100 μM) was added to the cells and incubated for 72 h. After completion of the incubation period, the medium was replaced by replaced by AlamarBlue™ Cell Viability Reagent (Thermo Fisher Scientific, Karlsruhe, Germany) at 10 % in cell media and incubated for 1 h. The degree of cell viability was determined by translating the blue non-fluorescent resazurin into pink-colored and fluorescent resorufin products by metabolically viable cells. After 1 h of incubation, the fluorescence was measured (Ex/Em 560/590 nm) using a plate reader (Fluostar Optima, BMG Labtech, Germany). Experiments were performed at least in quadruplicate, and all data were normalized with respect to the negative control (cell culture medium), which was considered 100 % metabolic activity. Nonlinear regression analysis was performed to determine the half-maximal inhibitory concentration (IC_{50}) using GraphPad Prism Software vs. 8.4.3 (GraphPad Software Inc.). The synergistic, additive, or antagonistic cytotoxic effects of PTX and VD_3 formulated as PTX+VD3S-PEG600 micelles were evaluated by the determination of the combination index (CI) as previously described in Ref. [56]. The IC_{50} values from the Alamar Blue assay were used to calculate the CI using the following equation:

$$CI = \frac{IC_{50}(X+Y)}{IC_{50}(X)} + \frac{IC_{50}(X+Y)}{IC_{50}(Y)} \quad (3)$$

where $IC_{50}(X)$ and $IC_{50}(Y)$ represent the IC_{50} value of PTX and VD_3 alone, respectively. $IC_{50}(X + Y)$ is the IC_{50} value of both drugs in combination. Values of $CI > 1$ indicate antagonistic effect, $CI = 1$ additive effect, and $CI < 1$ synergistic effect.

2.16. Construction of 3D cell culture models

BxPC-3 cells were harvested and suspended in the respective cell media at a density of 3×10^7 cells/mL after reaching 70%–80 % confluency. Collagen I (Col I) was extracted from rat tails as previously described [57]. The total protein content of Col I (17 mg/mL) was quantified by microBCA (Thermo Fisher Scientific, Karlsruhe, Germany) using Col I as a standard (OptiCol Rat Collagen Type I, no. MS18, Cell Guidance Systems). Then, 10 × DPBS (300 μL, pH~7.4) was added to the extracted Col I to obtain a final 1 × PBS (pH~7.4) concentration, safeguarding cell-friendly osmolarity. The pH of the Col I suspension was neutralized with NaOH 1M. To prepare 1 mL of the Col I pre-gel at 4 mg/mL, the neutralized Col I dispersion was mixed with 100 μL of cell suspension and made up to volume with cell culture medium to obtain a final cell density of 3×10^6 cells/mL. The resulting pre-gel was vortexed and incubated at 4 °C for 8 min. Subsequently, 25 μL of pre-gel was added to the 48-well plates and incubated at 37 °C for 15 min. Then, the cell culture medium was added on top of the recently formed hydrogel [52,54]. To study the cellular morphology of the hydrogels, the cells were stained with Alexa Fluor 488 phalloidin and DAPI using the same procedure described in **Section 2.14**.

2.17. In vitro cytotoxicity of paclitaxel-loaded micelles in 3D cell culture models

Cell-laden hydrogels were cultured for 3 days to enable BxPC-3 cell growth. The hydrogels were then incubated with free PTX, free VD_3, blank VD_3S-PEG_{600} micelles, and PTX+VD_3S-PEG_{600} micelles at different concentrations of PTX or equivalent (0.01, 1, 10, and 100 μM) for 72 h. Cell viability was determined using the Alamar Blue assay as previously described for 2D cell culture models in **Section 2.15.** Qualitative analysis of cytotoxicity after exposure to PTX+VD_3S-PEG_{600} micelles (equivalent concentration of PTX was 10 μM) was also evaluated using the LIVE/DEAD™ Viability/Cytotoxicity staining kit (Invitrogen, Carlsbad, USA) on the 3D PDAC cell culture models. Samples were processed according to the manufacturer's instructions. After 72h of cell-laden Col I hydrogels were prepared, they were washed with 1 × DPBS (pH7.4) and incubated (20 min at 37 °C) with a solution of green-fluorescent Calcein AM 2 μM (Ex/Em 494/517 nm) and red-fluorescent ethidium homodimer 4 μM (Ex/Em 517/617 nm) in 1 × DPBS (pH~7.4) to stain viable and dying cells, respectively. Subsequently, the hydrogels were washed with 1 × DPBS (pH7.4), and Z-stack images were acquired using a Confocal Laser Scanning Microscope (Leica TCS-SP5, Leica Microsystems). Image analysis was performed using Leica SP8 LAS X Life Science Microscope Software (Version 3.5.5, Leica, Germany) [55].

2.18. In ovo chorioallantoic membrane assay

The chorioallantoic membrane (CAM) tumor grafted model was used as an alternative to other *in vivo* models to study the antitumoral activity of PTX+VD_3S-PEG_{600} micelles against PDAC (BxPC-3 cells). This assay was performed as recently described [59] with slight modifications. Briefly, fertilized White Leghorn hen eggs (50–60 g, Coren, San Cibrao das Viñas, Spain) were cleaned with EtOH 70 %, and incubated at 37 °C and 60 % relative humidity (RH) with hand-rotation three times per day for 3 days. On embryonic development day (ED) 3, the pointed pole of the eggs was punctured using a 21-Gauge (G) needle (Braun Sterican®, Melsungen, Germany) and albumin (1–2 mL) was removed with a syringe to create an air hole for subsequent tumor inoculation. The puncture was sealed with tape and eggs were incubated in horizontal position. On ED 6, a small window (1 cm^2) was created into the egg shell and the presence of the embryo was confirmed before proceeding with the grafting of the tumor cell suspension on the CAM. The opened windows were properly covered with films to prevent contamination and drying out of the eggs. Then, a cell suspension in RPMI without FBS (20 μL containing 2×10^6 cells) was mixed with Matrigel® extracellular matrix components (40 μL, Corning, New York, USA) and deposited into a sterile silicone ring (Ø 3 mm) that was placed on the CAM. Eggs were kept for 30 min at RT to allow Matrigel® gelation. After a further incubation period of four days (ED 10), the eggs were randomly assigned to groups (n = 4) and treated with free PTX, free VD_3, VD_3S-PEG_{600} micelles, PTX+VD_3S-PEG_{600} micelles, and Abraxane® suspended in 10 μL of RPMI (equivalent concentration of PTX was 100 μM). All the eggs manipulation procedure was conducted maintaining sterile conditions and embryos that died before day 14 were excluded from further analysis. On ED 14, the eggs were withdrawn from the incubator and opened windows were further enlarged to make the tumor more accessible for macroscopical visualization analysis. Images of the tumor grafted CAM were acquired using a Leica M205 FCA fluorescence stereo microscope (Leica, Wetzlar, Germany) in brightfield to visualize the tumor growth. Then, embryos were sacrificed with 4 %(v/v) paraformaldehyde, and microtumors with adjacent CAM were excised. *Ex ovo* images were captured using the same stereo microscope to further assess the extent of vascular network and the effect of the PTX+VD_3S-PEG_{600} micelles on the inhibition of angiogenesis by vessel analysis using ImageJ software. After this step, the tumors were removed from the CAM and weighed. According to Directive 2010/63/EU, the CAM test is not considered as an animal experiment and therefore does not require ethical approval.

2.19. Hemolysis assay

Human blood was provided by the Galician Transfusion Center (ADOS) and obtained from anonymous healthy donors after obtaining written informed consent in agreement with Spanish legislation (Law 14/2007 on Biomedical Research). Whole blood was diluted with PBS (pH~7.4) to prepare a 2.5 % (v/v) blood suspension. Aliquots of diluted blood (900 μL) were added to the diluted (in PBS) blank and PTX-loaded VD_3S-PEG_{600} micellar formulations (100 μL; 0.001, 0.001, 0.01, 0.1, 1.0, 2.5, and 5 mg/mL), and VD_3-PEG_{2000} micellar formulations (100 μL; 5 mg/mL). Additionally, a PTX solution in EtOH (1 mg/mL) was prepared and added to the diluted blood to obtain a final PTX concentration of 0.1 mg/mL. After incubation for 60 min at 37 °C and 100 rpm in an orbital

shaker, samples were centrifuged at 700 g for 10 min. Supernatants were collected and each sample was individually placed (150 μL) in a 96-well plate in duplicate. Hemolytic activity was calculated as a function of the relative hemoglobin content released by the lysed erythrocytes. The hemoglobin present in the supernatant was determined by recording the absorbance (Abs) at 540 nm using a plate reader (Fluostar Optima, BMG Labtech, Germany). Maximum (100 %) hemolysis was obtained by adding 100 μL of Triton X-100 (positive control) to 900 μL of diluted blood, while minimum hemolysis was achieved by adding PBS aqueous solution (negative control) to 900 μL of diluted blood. All formulations were tested in triplicate, and the results are reported as mean ± standard deviation. The results expressed as hemolysis percentages were obtained using the following equation:

$$\text{Hemolysis}\ (\%) = \frac{\left(\text{Abs}_{\text{Sample}} - \text{Abs}_{\text{Negative control}}\right)}{\left(\text{Abs}_{\text{Positive control}} - \text{A}_{\text{bsNegative control}}\right)} \times 100\% \quad (4)$$

where $\text{Abs}_{\text{Sample}}$ represents the sample absorption value, $\text{A}_{\text{Negative control}}$ the negative control absorption value, and $\text{Abs}_{\text{Positive control}}$ the positive control absorption value.

2.20. HET-CAM assay

The hemocompatibility of blank VD_3S-PEG_{600} micelles and PTX+VD_3S-PEG_{600} micelles was also tested using the HET-CAM assay. After 8 days of incubation of the fertilized White Leghorn hen eggs (50–60 g, Coren, San Cibrao das Viñas, Spain) in a climatic chamber at 37 °C and 60 % RH, a small window of about 1 cm^2 was made on the eggshell to expose the CAM. Then, 200 μL of each formulation were directly poured on the CAM and 0.9 % NaCl and 0.1N NaOH solutions were used as negative and positive controls, respectively. CAM vessels were visually monitored for 5 min to assess the appearance of hemorrhage, vascular lysis, coagulation, hyperemia, or other changes in CAM vessels.

2.21. Statistical analysis

Statistical analysis was performed using GraphPad Prism Software vs. 8.4.3 (GraphPad software, Inc, La Jolla, CA) and sing IBM SPSS statistics 26.0 software (SPSS Inc., Chicago, IL, USA). All experiments were performed at least in triplicate and expressed as mean ± standard deviation. The data were assessed for normality by evaluating its distribution and performing normality tests (the Shapiro–Wilk ($n \leq 50$) and Kolmogorov–Smirnov ($n \geq 50$) tests). Statistical significance was

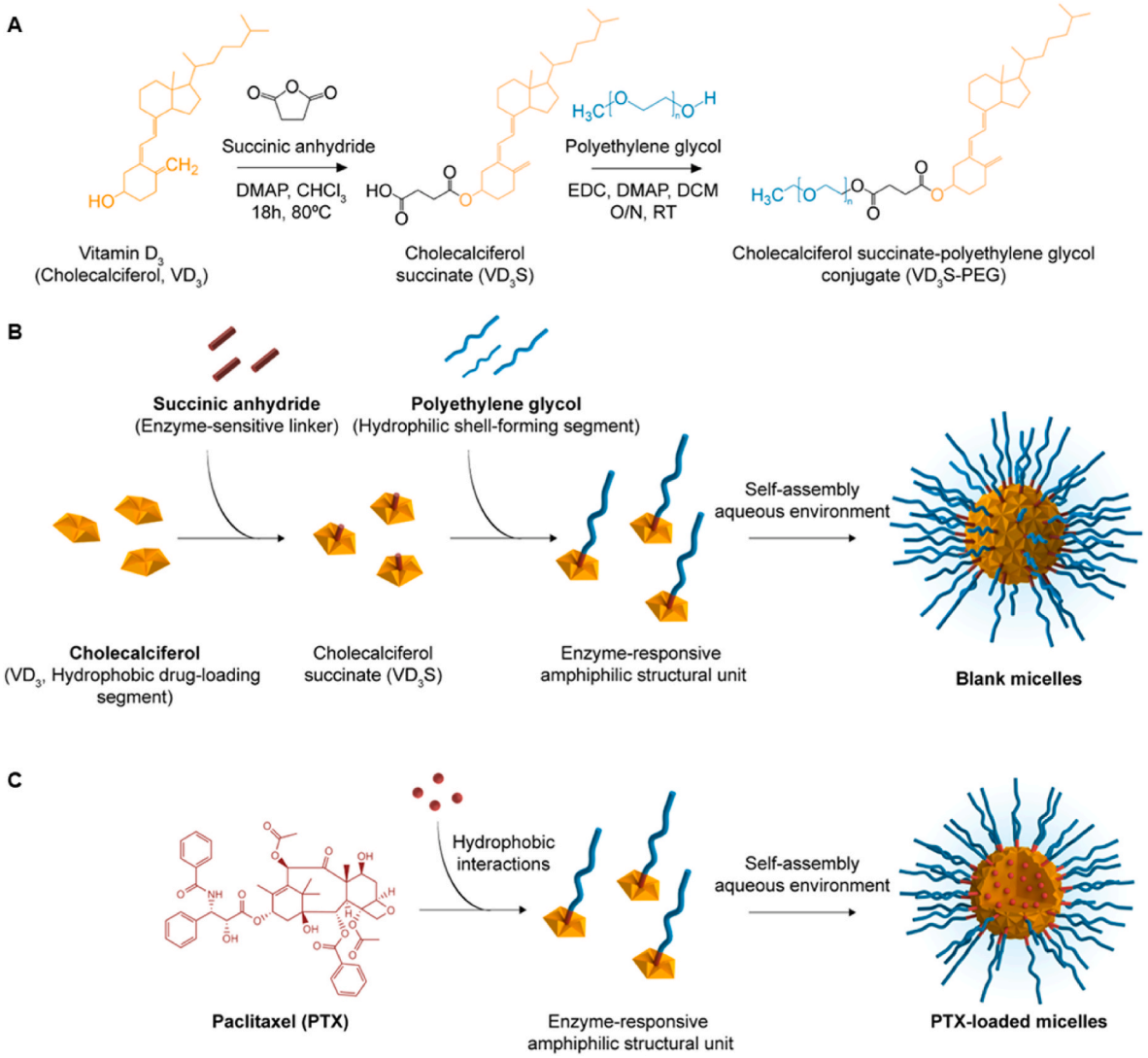

Fig. 1. (A) Two-step synthesis of VD_3S-PEG conjugate: Functionalization VD_3 with a succinate ester linker followed by the combination of VD_3S with PEG *via an* esterification reaction. **(B–C)** Schematic illustration showing the self-assembly of blank **(B)** and PTX-loaded **(C)** micelles.

determined using one-way analysis of variance (ANOVA), followed by the Tukey post hoc test when different groups were compared. A value of *p < 0.05 was considered statistically significant (*p < 0.05, **p < 0.005, ***p < 0.001 and ****p < 0.0001).

3. Results and discussion

3.1. Synthesis and characterization of cholecalciferol succinate-polyethylene glycol conjugate

The esterase-responsive VD_3S-PEG conjugates were synthesized using a simple two-step process (Fig. 2A). In the first step, the carboxylic acid derived from the succinic anhydride reacts with the hydroxyl (-OH) group of VD_3 to form the ester form of VD_3 succinate (VD_3S) through a

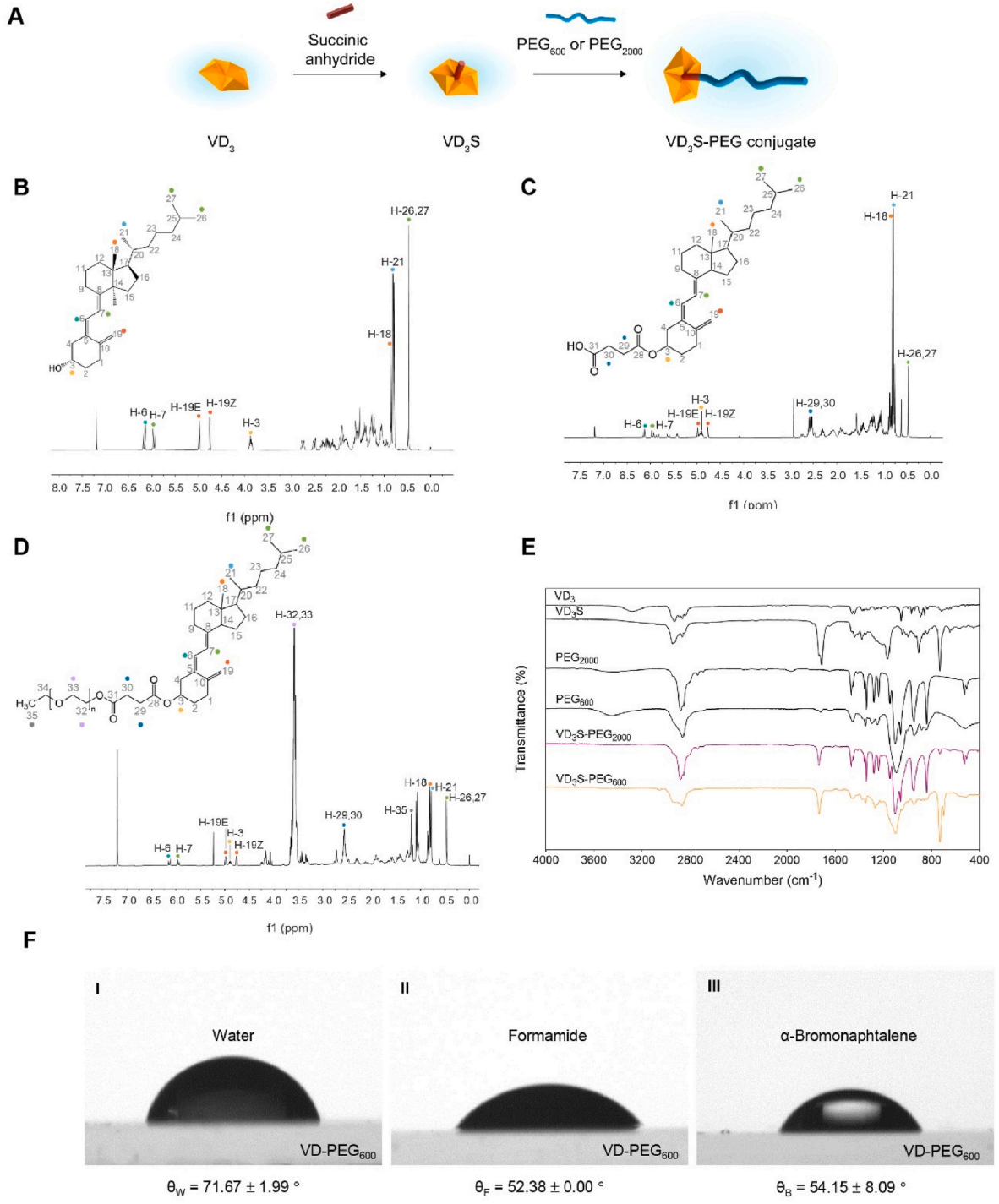

Fig. 2. Synthesis and characterization of VD_3S-PEG conjugates. **(A)** Schematic illustration of the construction of VD_3S-PEG conjugates. **(B)** ^1H NMR (300 MHz, $CDCl_3$) spectrum of VD_3. **(C)** ^1H NMR (300 MHz, $CDCl_3$) spectrum of VD_3S. **(D)** ^1H NMR (300 MHz, $CDCl_3$) spectrum of VD_3S-PEG_{600}. **(E)** FTIR spectra of VD_3, VD_3S, PEG_{2000}, PEG_{600}, VD_3S-PEG_{600}, and VD_3S-PEG_{600}. **(F)** Contact angle (in degrees) measured between (I) water (θ_W), (II) formamide (θ_F), (III) α-bromonaphthalene (θ_B), and VD_3-PEG_{600} conjugate flat surface. Values are expressed as mean ± standard deviation, n = 3.

condensation reaction known as esterification. Subsequently, the second step consists in the carbodiimide coupling of VD_3S with PEG_{600} or PEG_{2000}, yielding the VD_3S-PEG_{600} and VD_3S-PEG_{2000} conjugates. The detailed synthetic route for VD_3-PEG conjugates is shown in Fig. 1A. All reactions were carried out under an argon atmosphere and protected from light to avoid VD_3 oxidation. VD_3S-PEG conjugates were purified using column chromatography and characterized using ^{1}H NMR and FTIR spectroscopy, as described in the Supplementary Material file. In the ^{1}H NMR spectrum of VD_3 (Fig. 2B and Fig. S1), the majority of proton resonances of the of the steroid skeleton were overlapped between δ 2.5 ppm and δ 1.0 ppm, making it impossible to correctly identify them. However, it was possible to identify some characteristic and well-defined peaks of VD_3 in the δ 6.5–2.5 ppm region. Particularly, signals from vinylic protons appeared as two doublets at δ 6.23 ppm and δ 6.03 ppm. In turn, signals from geminal vinylic protons occurred at δ 5.08–5.01 ppm region. The proton adjacent to the -OH group bonded to the three-membered A-ring was observed as multiplet around δ 3.94 ppm. Furthermore, the singlet at 0.54 ppm and three doublets at δ 0.92 ppm, δ 0.88 ppm, and δ 0.82 ppm were assigned as protons of methyl groups (–CH_2). The ^{1}H NMR spectrum of VD_3S (Fig. 2C and Fig. S2) showed similar signals as observed in the spectra of VD_3 except succinyl methylene (–CH_2) protons at δ 2.6–2.7 ppm region, suggesting the reaction between VD_3 and succinic anhydride. Besides, the peak of the alcohol hydroxyl proton of VD_3 was deshielded and absorbed in the δ 4.97 ppm region possibly due to the electron-withdrawing effect of the formed carboxylic acid. The chemical shift at δ 3.3 ppm region may have resulted from the presence of residual unreacted succinic anhydride, which was further removed by a final column purification step. The ^{1}H NMR spectra of VD_3S-PEG conjugates (Fig. 2D– Figs. S5 and S6) were the combination of ^{1}H NMR spectra of both VD_3S and PEG (Figs. S3 and S4), showing the characteristic ethylene protons of PEG chain at δ 3.55–3.75 ppm region with several characteristic signals of VD_3S [60]. The absence of the characteristic peak of succinic anhydride around δ 3.3 ppm indicated that the unreacted succinic anhydride was successfully removed from VD_3S-PEG conjugates by column chromatography. In addition, the successful preparation of VD_3S and VD_3S-PEG conjugates was also evidenced by ^{13}C NMR experiments (Figs. S7–S9). Apart from the signals featured by VD_3, the ^{13}C NMR spectra of VD_3S-PEG conjugates showed the characteristic signals of the carbonyl carbons belonging to the formed ester linker in the δ 160–180 ppm region. The PEG moiety was easily identified by its signal centered around δ 70 ppm. Complementarily, FTIR was used to better describe the properties of the synthesized VD_3S- $PEG_{600,}$ and VD_3S-PEG_{600} and their respective structural elements (i.e., VD_3, VD_3S, PEG_{600}, and PEG_{2000}). The characteristic spectra of all compounds are shown in Fig. 2E. The VD_3 spectrum (Fig. S10) was characterized by a large and broad O-H stretching absorption band centered around 3300 cm^{-1}, arising from the OH group. All alkyl groups, either -CH_2 or -CH_3 groups, gave rise to absorption peaks in the 2800–3000-cm^{-1} region that were associated with C-H stretching vibrations. In addition, absorption bands arising from C-C double bonds of the cis-triene configuration (seco B-ring) occurred in the 1620-1680 cm^{-1} region. In the spectrum of VD_3S (Fig. S11), C-H stretching vibrations were overlapped by a strong and broad absorbance in the 2500–3600-cm^{-1} region, suggesting the presence of an OH group arising from a carboxylic acid. Strong peaks around 1710–1780 cm^{-1} were consistent with this finding, since they could arise from a carbonyl group (C=O) of the ester linkage or the terminal carboxylic acid of VD_3S. Besides, the presence of C-O stretching absorption bands in the range 1000–1260 cm^{-1} were in according with this. Conversely, VD_3 did not present the strong peak characteristic of the C=O stretching band. Collectively, the differences between VD_3 and VD_3S spectra indicated that succinic anhydride ring opened during the reaction with the -OH group of VD_3 forming an ester and leaving a free carboxylic group. Additionally, the strong C=O stretching band typically featured by the succinic anhydride in the 1820–1870 cm^{-1} region was not observed in the VD_3S spectrum. This suggests that a significant amount of the unreacted succinic anhydride was removed from VD_3S before the conjugation with PEG of different molecular weights (600 Da and 2000 Da). Regarding the spectra of PEG_{600} (Fig. S12) and PEG_{2000} (Fig. S13), both presented a large and broad O-H stretching absorption peaks of the terminal OH groups in the 3200–3650-cm^{-1} region. The bands observed at approximately 2865 cm^{-1} for PEG_{600} and 2881 cm^{-1} were attributed to the C–H stretching vibrations of -CH_2 groups. The absorption at 1454 cm^{-1} for PEG_{600} and 1466 cm^{-1} for PEG_{2000} were designated to the C–H bending vibrations of -CH_2 groups. Asymmetrical bending vibrations of –CH_3 groups were also present. Additionally, the characteristic backbone constituent ether groups of both types of PEG_{600} and PEG_{2000} gave rise to symmetrical C-O-C stretching vibrations at 1093 cm^{-1} and 1101 cm^{-1}, respectively. Moreover, the bands at 1248 cm^{-1} for PEG_{600} and 1239 cm^{-1} for PEG_{2000} were attributed to the C–O stretching vibration. In the spectrum of VD_3S-PEG conjugates (Figs. S14 and S15), the appearance of characteristic –C-O-C ether stretching vibrations at 1099 cm^{-1} for VD_3S-PEG_{600} and 1102 cm^{-1} for VD_3S-PEG_{600} and disappearance of the broad O-H stretching absorption peaks confirmed a successful conjugation of the terminal carboxyl group of VD_3S with the OH of PEG_{600} and PEG_{2000} *via* esterification reaction. Collectively, all the aforementioned findings demonstrated that VD_3S-PEG conjugates were successfully synthesized.

The contact angles of three different solvents (water, formamide, and α-bromonaphtalene) were measured to gain insights into the hydrophilicity of the VD_3-PEG_{600} conjugate. The water contact angle found for VD_3-PEG_{600} conjugate was 71.67 ± 1.99° (Fig. 2F), meaning it can be considered as a hydrophilic surface. Nevertheless, water contact angle measurements of amphiphilic conjugates tend to overestimate their water solubility when the hydrophilic segment is oriented toward the surface layer [61]. The interfacial tension components determined for the VD_3-PEG_{600} conjugate, namely the Lifshitz-van der Waals component (γ_S^{LW}), the electron acceptor (γ_S^+) and electron donor (γ_S^-) parameters were estimated to be 27.91, 2.01 and 10.88 mJ/m^2, as described in the Supplementary Material file. Accordingly, the surface energy value obtained for VD_3-PEG_{600} conjugate was around −27.98 mJ/m^2, suggesting a hydrophobic nature ($\Delta G_{SW}^{TOT} < 0$ mJ/m^2 indicates hydrophobicity). The value of apolar component (ΔG_{SW}^{LW}) was around −0.75 mJ/m^2, while the value obtained for apolar component (ΔG_{SW}^{AB}) was around −27.23 mJ/m^2. The lowest value for the surface apolar component suggests that VD_3-PEG_{600} has a higher affinity for polar liquids than for apolar liquids. Additionally, the VD_3-PEG_{600} conjugate presents predominantly an electron donor character (high γ_S^+ values, 10.88 mJ/m^2), with low electron acceptor ability (low γ_S^- values, 2.01 mJ/m^2), due to the presence of oxygen lone pair electrons (electron-donating oxygens) in the PEG segment. Collectively, these results indicate that the VD_3-PEG_{600} conjugate is moderately hydrophobic due to the presence of the highly hydrophobic VD_3, which is characterized by a broken bond in the B-ring of the four-ring steroid core (seco-steroid). The contact angles of formamide (52.38 ± 0.00°) (Fig. 2FII) and α-bromonaphtalene (54.15 ± 8.09°) (Fig. 2III) corroborated the moderate hydrophobicity of the VD_3-PEG_{600} conjugate.

The self-assembly properties of the VD_3-PEG_{600} conjugate were investigated using pyrene as the hydrophobic fluorescence probe. Upon interacting with micelles, pyrene preferentially moved from the aqueous environment to the hydrophobic core of the VD_3-PEG_{600} micelles and underwent a bathochromic shift (red shift) on the maximum of the emission spectrum emission spectrum from 323 nm to 334.5 nm occurred. The effect of VD_3-PEG_{600} concentration on the emission spectra of pyrene is shown in Fig. S21B. The CMC value of the VD_3-PEG_{600} conjugate (i.e., the minimum concentration required to maintain the micellar structure), estimated from the plot of the ratio of the first ($I_{334,5}$) to the third (I_{323}) vibronic peak of pyrene, was 103.58 μg/mL (Fig. S21C). This value was higher than the CMC value reported for the VD-PEG_{2000} conjugate (Table 2) [39], indicating that the hydrophilic/hydrophobic ratio determines the CMC value. This trend has been

Table 2
Molecular weight (MW) and critical micelle concentration (CMC) of VD_3S-PEG conjugates used to prepare VD_3S-PEG micelles.

Conjugate	MW of the conjugate (g/mol)	MW of PEG chains (Da)	Hydrophilic/hydrophobic ratio[a]	CMC (μg/mL)
VD_3S-PEG_{600}	1084	600	385/600	103.58[b]
VD_3S-PEG_{2000}	2484	2000	385/2000	89.00[c]

[a] Block molecular weight ratio of VD_3S-PEG in conjugates.
[b] CMC of VD_3S-PEG_{600} determined by the fluorescence probe method (Section 2,6).
[c] CMC of VD_3-PEG_{2000} at 25 ± 2 °C in PBS (pH~7.4) from fluorescence probe method [39].

described in previous studies [58,59]. Therefore, both conjugates can self-assemble at low CMC, which is advantageous for the solubilization of poorly water-soluble drugs without the dilution effect after administration in the blood circulation (Fig. S21A). In addition, the CMC of both VD_3-PEG conjugates was inferior to that reported for the common D-alpha-tocopherol polyethylene glycol succinate (TPGS) (ca. 200 μg/mL) [55,59], suggesting higher thermodynamic stability [22,60].

3.2. Preparation and characterization of blank and paclitaxel-loaded micelles

Considering that the VD_3S-PEG_{600} and VD_3S-PEG_{2000} conjugates were moderately hydrophobic and did not dissolve directly in PBS, the hydrophobic chemotherapeutic agent PTX and VD_3S-PEG conjugates were first co-dissolved in EtOH (Fig. 3A). The obtained dispersion was then slowly added (dropwise addition) into the PBS solution, which was used as a nonsolvent for VD_3S-PEG conjugates, to initiate the self-assembly process [49]. After solvent evaporation overnight, self-assembled PTX+VD_3S-PEG micelles were obtained, driven by the steric repulsion of the hydrophilic PEG chains in the shell and stretching of the hydrophobic VD_3 segment in the core [22,60]. The encapsulation of the hydrophobic small molecules of PTX into the core of the micelles could be primarily driven by hydrophobic interactions with the VD_3 segments (Fig. S16), which could further stabilize the micellar structure in the aqueous environment [66]. Free PTX that was not loaded into the micelles and the unassembled VD_3S-PEG conjugate was removed by filtration.

During the preparation of micelles, EtOH was selected because it is a well-accepted organic solvent for drug formulations owing to its low toxic potential (Class 3 solvent) [67]. Besides, the particle size of

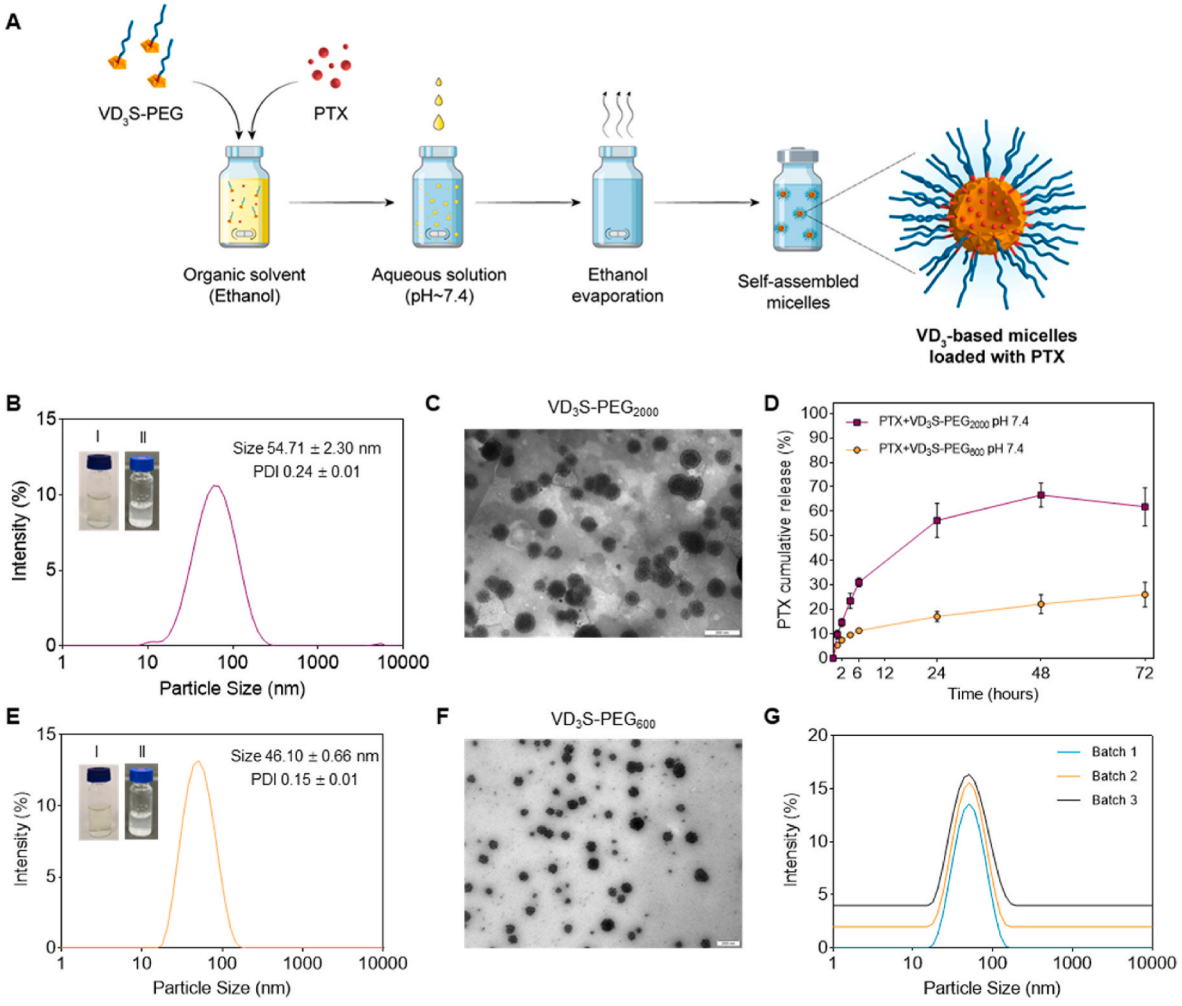

Fig. 3. Preparation and characterization of VD_3S-PEG micelles for efficient intracellular delivery of PTX. **(A)** Schematic illustration of PTX-loaded micelle preparation using the solvent evaporation method. **(B,E)** Particle size distribution by intensity (%) at 25 ± 2 °C for micelles composed of **(B)** VD_3S-PEG_{2000} and **(E)** VD_3S-PEG_{600} at 50 mg/mL after loading with PTX at 1 mg/mL. Inset: Macroscopic appearance of PTX+VD_3S-PEG micelles. **(C,F)** Representative TEM micrograph obtained from **(C)** blank VD_3S-PEG_{2000} (25 mg/mL) and **(F)** blank VD_3S-PEG_{600} (25 mg/mL) micelles (scale bar: 200 nm). **(D)** Release profile of PTX from VD_3S-PEG_{2000} or VD_3S-PEG_{600} micelles in PBS at pH 7.4, mimicking normal physiological conditions. **(G)** Particle size distribution by intensity (%) of PTX+VD_3S-PEG_{600} micelles at a ratio of 50:1 (w/w), prepared from three different batches of micellar formulations. All formulations shared comparable size distribution.

micelles depends on the chosen organic solvent, and EtOH usually leads to small micelles (<60 nm) due to the low interfacial tension between the hydrophobic segment and the solvent [62]. The ethanolic solution was added dropwise to the PBS medium (pH~7.4) either manually (ca 1 drop/5s) or using a syringe pump (0.15 mL/min) to investigate their effect on the particle size and polydispersity index (PDI) of the micelles. The PDI is a dimensionless measure of the broadness of the particle size distribution, where a PDI< 0.2 is indicative of monodisperse particle size distribution (Figs. S23A and D). Filtered blank VD_3S-PEG_{2000} micelles presented multiple populations in the intensity distribution at 25 °C (Fig. S23B), but monomodal distribution by number (Fig. S23C), which suggested that most particles had the same particle size and the multiple populations could be due to the formation of some aggregates [68]. These results indicate that the molecular weight of the VD_3S-PEG conjugates can affect the polydispersity and particle size of the micelles. The analysis of the particle size of filtered blank VD_3S-PEG_{600} micelles in PBS (pH~7.4) by intensity distribution at 25 ± 2 °C showed highly monodispersed micelles prepared using both methods (Fig. S23E). These blank micelles presented a particle size ranging from 21.64 ± 0.24 nm to 28.20 ± 0.11 nm and a PDI comprised between 0.05 ± 0.01 and 0.17 ± 0.02 (Table 3). Overall, no significant differences were observed in the particle size, PDI, and ZP of VD_3S-PEG_{600} and VD_3S-PEG_{2000} micelles prepared using the two dropwise addition methods. Therefore, the infusion/syringe pump was chosen for further studies because it minimized the variation introduced by the operator.

Several factors may affect the particle size, morphology, and, ultimately, the solubilization efficiency of micelles in solution, including **(i)** structural parameters of the VD_3S-PEG conjugate (e.g., molecular mass of the segments), **(ii)** VD_3S-PEG concentration, and **(iii)** environmental parameters such as temperature, ionic strength, and pH [69]. Therefore, PTX+VD_3S-PEG micelles were prepared using different VD_3S-PEG conjugate:PTX mass ratios (25:5, 25:1.2, 25:1, and 50:1w/w) to identify the formulation with the most suitable properties for use in further studies. PTX+VD_3S-PEG_{2000} micelles (F_1) at a VD_3S-PEG conjugate:PTX ratio of 25:5 (w/w) at 25 ± 2 °C presented bimodal size distributions (Fig. S24A and **S24B)**, and PTX aggregates might be attributed to the small peak around 5400 nm (Fig. S24C). These observations indicate that PTX was not successfully incorporated into the VD_3S-PEG_{2000} micelles. In turn, the particle size of VD_3S-PEG_{600} micelles at a VD_3S-PEG conjugate:PTX ratio of 25:5 (w/w) (F_2) increased to 46.77 ± 0.21 nm after encapsulating PTX molecules within micelles (Table 3). This indicates that PTX was successfully incorporated into the VD_3S-PEG_{600} micelles, which stretched the structure of the micelles. Decreasing the VD_3S-PEG conjugate:PTX ratio to 25:1.2 (w/w) resulted in VD_3S-PEG_{600} micelles (F4) with a large particle size (75.30 ± 2.67 nm) and a very high PDI (0.55 ± 0.01) but did not significantly change the particle size of micelles prepared with VD_3S-PEG_{2000} conjugate (25.11 ± 0.29) (F3). This high PDI value indicates a broad range of particle sizes, low stability, and possible micelle aggregation. The particle size by intensity of filtered micelles before and after PTX loading was monomodal (Figs. S24A and D), and multiple populations detected in the distribution by number could be due to the non-encapsulated PTX remaining in the formulation (Figs. S24B and E). Additionally, formulations prepared using a VD_3S-PEG conjugate:PTX ratio of 25:5 (w/w) presented an opalescent appearance with PTX-precipitated particles, which was necessary to either decrease the amount of PTX or increase VD_3S-PEG concentration. Increasing the VD_3S-PEG conjugate:PTX ratio to 50:1 (w/w) allowed the formation of PTX + VD_3S-PEG_{2000} (F_7) and PTX+VD_3S-PEG_{600} micelles (F_8) with larger particle sizes and/or lower PDI (<0.2) than the VD_3S-PEG conjugate:PTX ratio of 25:1 (w/w) micelles (Fig. 3), without the presence of precipitated PTX particles (Table 3). These observations suggested that PTX was successfully incorporated into VD_3S-PEG_{600} and VD_3S-PEG_{2000} micelles with a narrow size distribution. The low PDI value indicated the homogeneity and high stability of the self-assembled micelles. PTX+VD_3S-PEG_{600} micelles at a ratio of 50:1 (w/w) also exhibited minimal batch-to-batch variation (Fig. 3G), with an average particle size of *ca.* 47.67 ± 0.09 nm and PDI values close to 0.17 ± 0.02, as assessed by DLS. All VD_3S-PEG micelles presented a particle size less than 100 nm (Table S4), making them promising drug delivery systems to not only evade the RES but also to improve the distribution, penetration, and tumor accumulation of chemotherapeutic agents in poorly permeable tumors such as PDAC [19]. Moreover, the particle size of VD_3S-PEG micelles superior to 10 nm can substantially reduce the renal clearance of the loaded PTX (threshold for glomerular filtration in kidney <6 nm) and, ultimately, can prolong the half-life of PTX *in vivo* [60]. Considering that the smallest values for particle size and PDI were achieved for a VD_3S-PEG conjugate:PTX ratio of 50:1 (w/w), this proportion was fixed to prepare PTX+VD_3S-PEG micelles for further studies.

Globally, all PTX+VD_3S-PEG micelles presented pH values close to the pH of the PBS (pH~7.4) in which they were prepared (pH values ranging between 7.27 ± 0.03 and 7.95 ± 0.02), occurring a slight decrease in pH after PTX addition. Besides, all PTX+VD_3S-PEG micelles exhibited a ZP in the negative range but close to neutrality (ranging from −11.19 ± 0.90 mV to 1.11 ± 0.77 mV) confirming the presence of PEG chains in the shell of the micelles (Table 3). This is an important feature because positively charged nanoplatforms are rapidly sequestered in the liver, spleen, and lungs, whereas neutral or slightly negatively charged systems exhibit prolonged circulation in the bloodstream [70]. Moreover, the steric repulsive effect of PEG may prevent the aggregation of polymeric micelles *in vivo* as well as during storage.

The morphology of the prepared blank micelles was studied by TEM, which revealed that the two VD_3S-PEG conjugates could readily self-assemble to form spherical micelles. This morphology was favored

Table 3
Characterization of blank (B) and PTX-loaded (F) micelles. The mean particle size, polydispersity, polydispersity index (PDI), and zeta potential (ZP) of blank and PTX-loaded micelles, and the encapsulation efficiency (EE) and drug loading content (DL) of PTX-loaded micelles prepared with VD_3S-PEG_{600} or VD_3S-PEG_{2000}. Samples were analyzed at 25 ± 2 °C (Results shown as the mean ± standard deviation, n = 4). ND-Not determined.

Formulation code	Particle size (nm)	PDI	ZP (mV)	pH	EE (%)	DL (%)
B_1	25.67 ± 3.25	0.23 ± 0.10	−4.73 ± 2.51	7.48 ± 0.24	–	–
B_2	28.20 ± 0.11	0.13 ± 0.01	−3.00 ± 1.29	7.32 ± 0.01	–	–
B_3	36.79 ± 3.49	0.47 ± 0.06	0.62 ± 1.32	7.87 ± 0.01	–	–
B_4	21.64 ± 0.24	0.05 ± 0.01	1.11 ± 0.77	7.95 ± 0.02	–	–
B_5	21.97 ± 7.68	0.37 ± 0.12	−1.67 ± 1.90	7.23 ± 0.03	–	–
B_6	27.15 ± 0.15	0.17 ± 0.02	−1.19 ± 1.20	7.44 ± 0.02	–	–
F_1	24.16 ± 4.00	0.35 ± 0.03	−3.60 ± 1.75	7.20 ± 0.03	ND	ND
F_2	46.77 ± 0.21	0.19 ± 0.01	−11.19 ± 0.90	7.62 ± 0.09	ND	ND
F_3	25.11 ± 0.29	0.27 ± 0.02	−1.69 ± 1.86	7.73 ± 0.01	22.99 ± 0.52	3.68 ± 0.02
F_4	75.30 ± 2.67	0.55 ± 0.01	1.04 ± 1.18	7.27 ± 0.03	22.02 ± 0.26	3.73 ± 0.01
F_5	25.11 ± 0.29	0.16 ± 0.02	−0.95 ± 0.98	7.87 ± 0.01	18.58 ± 0.04	3.21 ± 0.01
F_6	68.91 ± 0.24	0.25 ± 0.05	−7.38 ± 1.97	7.93 ± 0.06	25.78 ± 0.05	2.85 ± 0.02
F_7	54.71 ± 2.30	0.24 ± 0.01	−4.36 ± 0.68	7.88 ± 0.02	51.20 ± 0.60	1.02 ± 0.01
F_8	46.10 ± 0.66	0.15 ± 0.01	−7.23 ± 1.62	7.80 ± 0.01	58.48 ± 3.40	1.07 ± 0.07

because the hydrophilic segment (shell) was longer than the hydrophobic segment (core). The cores of both VD_3S-PEG_{600} and VD_3S-PEG_{2000} micelles were stained with phosphotungstic acid and visualized as uniform black dots (Fig. 3C–F). The particle size of micelles observed under TEM was found to be slightly larger than that measured by DLS, probably due to a certain expansion of the micelles when exposed to the high-energy electron beam in TEM [49]. Additionally, a dense PEG shell in the VD_3S-PEG_{2000} micelles is clearly observed in the TEM images (Fig. S26E). Overall, the assembled micelles feature highly ordered macromolecular structures with segregated hydrophobic compartments in the core, surrounded by a hydrophilic shell on the outer surface of the micelle, which confines the overall micelle architecture.

3.3. Stability of paclitaxel-loaded micelles

Micelle structural stability, with respect to particle size and PDI values, as well as the absence of PTX precipitation, was addressed under different long-term storage conditions and in the presence of distinct biorelevant media. For long-term stability, undiluted PTX+VD_3S-PEG micelles were stored at 4 ± 2 °C or 25 ± 2 °C, and particle size was measured each week for 4 weeks. The particle size of the PTX+VD_3-PEG_{2000} micelles did not change significantly at 4 °C, but the PDI values slightly increased after the second week of storage, suggesting that micelle aggregation may have started to occur (Fig. 4A). In turn, the size and PDI values of PTX+VD_3S-PEG_{600} micelles remained stable, and no PTX precipitation occurred during storage at 4 ± 2 °C and 25 ± 2 °C, demonstrating the ability of the PEG_{600} hydrophilic shell to avoid micelle aggregation (Fig. 4B and C). Therefore, PTX+VD_3S-PEG_{600} micelles were confirmed to be highly stable for at least one month at the *in-use* temperatures that could be found in a hospital setting (4 °C and 25 °C). Further characterization of PTX+VD_3S-PEG_{600} micelles indicated high stability after exposure to simulated normal body temperature (37 ± 2 °C), with particle size and PDI values resembling the original values and without any precipitation (Fig. 4B and C). The stability of PTX+VD_3S-PEG_{600} micelles was also confirmed after dilution (1:1 v/v) with physiologically relevant media (PBS, FBS, RPMI 1640 cell culture medium, and human blood plasma), further supporting their stability in physiological environments. The observed slight increase in particle size after 24 h at 37 ± 2 °C may be due to protein deposition on the surface of the micelles (Fig. 4E and F). Overall, PTX+VD_3S-PEG_{600} micelles were quite stable, exhibited good dispersibility, and showed no visible precipitation in any of the biorelevant media.

3.4. Drug loading and encapsulation efficiency

HPLC chromatographic conditions for PTX quantification were optimized in terms of run time (6–20 min), flow rate (0.5–1.0 mL/min), mobile phase composition and ratio (acetonitrile/water 80:20 to 60:40) (Fig. S17). After several chromatographic runs, a mobile phase consisting of acetonitrile: water (60:40 v/v) was optimized at a flow rate of 1 mL/min, using a run time of 10 min. Under the described chromatographic conditions, no interference was observed at the retention time of PTX (Figs. S18 and S19), all peaks were well defined, and PTX was quantified using a UV detector set at 227 nm. The highest DL (%) was 3.73 %, which resulted from the VD_3S-PEG_{600} conjugate:PTX ratio of 25:1.2 (w/w) (Table 3). This low DL content might be related not only to the bulky nature of PTX (MW 853 g/mol) but also to undesired PTX self-aggregation due to nonspecific hydrophobic interactions among free PTX molecules. The EE (%) values of PTX+VD_3S-PEG micelles ranged from 18.58 % to 58.48 %. The highest EE (%) was obtained for the VD_3S-PEG_{600} conjugate:PTX ratio of 50:1 (w/w) (Table 3). This was translated to an increase in the aqueous solubility of PTX from 0.3 μg/mL to 547.8 μg/mL (i.e., 1800-fold increase in PTX solubility).

3.5. In vitro paclitaxel release in media of different pH

Release tests were performed in PBS containing 0.5 % polysorbate 80 (Tween® 80) to overcome the low aqueous solubility of PTX (Abouelmagd et al., 2015) and to avoid artifact plateaus and saturation of the medium [23,71]. Polysorbate 80 did not interfere with HPLC chromatograms (Fig. S17). The release kinetics of PTX from VD_3S-PEG micelles was first measured in medium mimicking physiological conditions (pH7.4) (Fig. 3D and Table S5). VD_3S-PEG_{600} micelles released PTX more slowly than VD_3S-PEG_{2000} micelles (20 % PTX *vs.* 66 % PTX at 48 h) indicating different attractive drug-drug and drug/VD_3S-PEG conjugate interactions (Fig. S16 and Table S2). The release behavior of

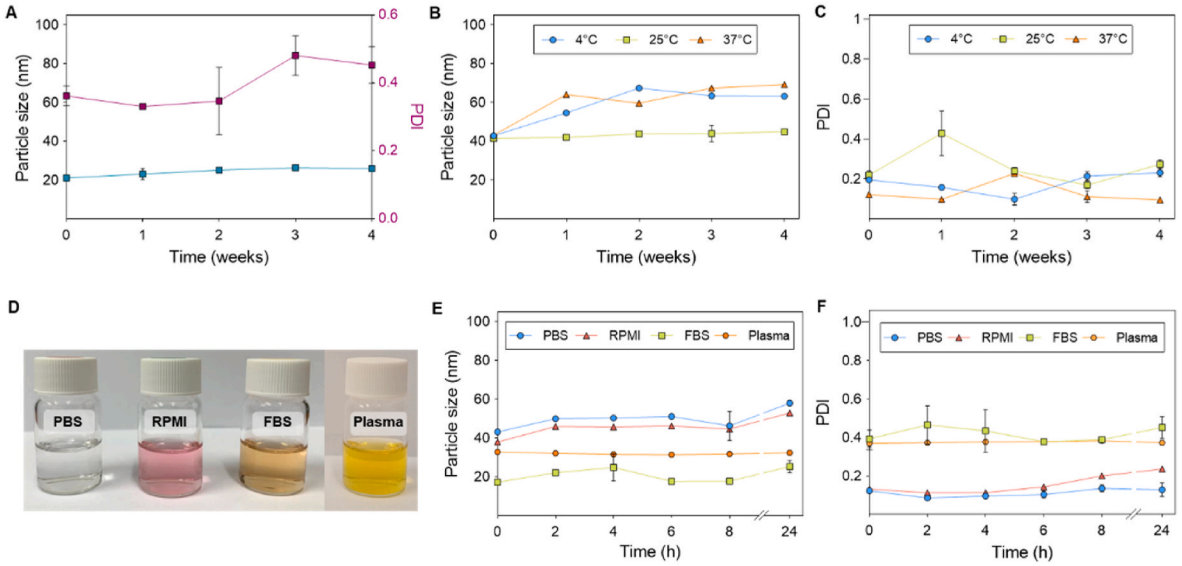

Fig. 4. Stability of PTX+VD_3S-PEG micelles. Representative DLS results indicated the stability of the PTX+VD_3S-PEG micelles after long-term storage (4 weeks). **(A)** Stability studies of PTX+VD_3S-PEG_{2000} micelles at ratio of 50:1 (w/w) stored at 4 ± 2 °C by plotting average particle size (nm) and PDI over 4 weeks. Stability studies of micelles composed of PTX+VD_3S-PEG_{2000} micelles at ratio of 50:1 (w/w) stored at 4 ± 2 °C by plotting average particle size (nm) **(B)** and PDI **(C)** over 4 weeks. **(D)** The appearance of blank VD_3S-PEG_{600} micelles after incubation in different biorelevant media at 37 °C. **(E,F)** Time-dependent colloidal stability of PTX+VD_3S-PEG_{600} micelles at ratio of 50:1 (w/w) in PBS, RPMI cell culture medium, FBS, and human blood plasma at 37 °C (Results shown as the mean ± standard deviation, n = 4).

VD_3S-PEG_{2000} micelles was in agreement with previous studies, which found that these micellar systems released approximately 90 % of their payload in 12 h [39]. Even after 72 h, VD_3S-PEG_{600} micelles released only about 31 % PTX, confirming the compact structure of these micelles due to strong interactions between PTX and VD_3S-PEG_{600}.

The pH sensitivity of the PTX+VD_3-PEG_{600} micelles was screened at different pH values, simulating normal pancreatic juice conditions (pH~8.2) and acid pancreatic TME (pH~6.5). The release pattern of PTX was similar, regardless of the change in pH, with an initial slow release (3.55 % at pH~6.5, 5.33 % at pH~7.4, and 3.85 % at pH~8.2 in 1 h), followed by a sustained release. The release of PTX after 48 h was 20.92 % at pH~6.5, 22.17 % at pH~7.4, and 20.35 % at pH~8.2. The cumulative release of PTX from VD_3S-PEG_{600} micelles after 216 h was 38.93 % at pH~6.5, 39.76 % at pH~7.4, and 26.03 % at pH~8.2 (Fig. 5C). The release results clearly indicate that the size of the PEG chain determines the release kinetics, since micelles possessing a lower hydrophilic fraction exhibit slower release rates than micelles with a higher hydrophilic fraction [64]. Therefore, short- and long-term drug release profiles could be obtained by tuning the length of the PEG used to prepare the VD_3S-PEG conjugates, where VD_3S-PEG_{2000} micelles could be an option for obtaining a fast release and VD_3S-PEG_{600} for a sustained release. Additionally, PTX release profiles from VD_3S-PEG_{600} micelles did not depend on pH, suggesting that these micelles could avoid premature drug release in the blood circulation. However, in more acidic environments or in the presence of enzymes, ester bonds may be partially hydrolyzed, which can disrupt the VD_3S-PEG conjugate. In fact, VD_3S-PEG_{600} and VD_3S-PEG_{2000} conjugates contain a *succinate* ester linker that imparts enzyme-responsiveness and disassembly of PTX+VD_3S-PEG micelles to promote drug release. This issue is addressed as follows.

3.6. Enzyme responsiveness of paclitaxel-loaded micelles

PTX+VD_3S-PEG_{600} and PTX+VD_3S-PEG_{2000} micelles are expected to prevent the uncontrolled release of PTX before reaching the desired target cell and to dissociate in the presence of esterase ubiquitously present in PDAC tissues to release PTX (Fig. 5A). Accordingly, the *in vitro* sensitivity of PTX+VD_3S-PEG_{600} micelles to enzymatic hydrolysis was analyzed in the presence of an esterase from the porcine liver. The isoenzyme PLE was used as an efficient non-specific carboxylic ester hydrolase to trigger the enzymatic hydrolysis of the VD_3S-PEG_{600} conjugate, as previously reported for related drug delivery systems [15,24]. After 24 h of incubation at 37 ± 2 °C, the change in particle size of PTX-loaded micelles was evaluated by DLS (Fig. 5B–E) and TEM (Fig. 5F). PTX+VD_3S-PEG micelles presented a particle size around 34.99 ± 0.20 nm by DLS and a narrow particle size distribution at pH~7.4 or pH~6.5 without PLE after incubation at 37 °C for 24 h (Fig. 5B–E). As the pH decreased from 7.4 to 6.5 in the presence of PLE (mimicking the mildly acidic environment in PDAC tissues supplemented with 50 U PLE/mL), PTX+VD_3S-PEG micelles cracked and showed a significant increase in particle size and high polydispersity. Compared to the PTX release profiles in absence of PLE (<30 % PTX released in 72 h), in media containing 50 U/mL of PLE, PTX release accelerated and was found to be 86 % at pH~6.5 and 62 % at pH~7.4 after 72 h of incubation (Fig. 5C). Additionally, Fig. 5I shows the effect of PLE on VD_3 release from VD_3S-PEG_{600} micelles. In the absence of PLE, VD_3S-PEG_{600} micelles remained stable for a long period with almost no VD_3 release. Approximately 97 % of VD_3 was released when VD_3S-PEG_{600} micelles were incubated with PLE at pH~6.5 for 72 h. The presence of PLE caused the massive release of VD_3 from VD_3S-PEG_{600} micelles due to enzyme responsiveness. This capacity offered by VD_3S-PEG_{600} micelles can conduct an efficient enrichment of VD_3 and PTX in cancer cells and improve the antitumor activity effect of both therapeutic agents, facilitating the long circulation of the micelles *in vivo*

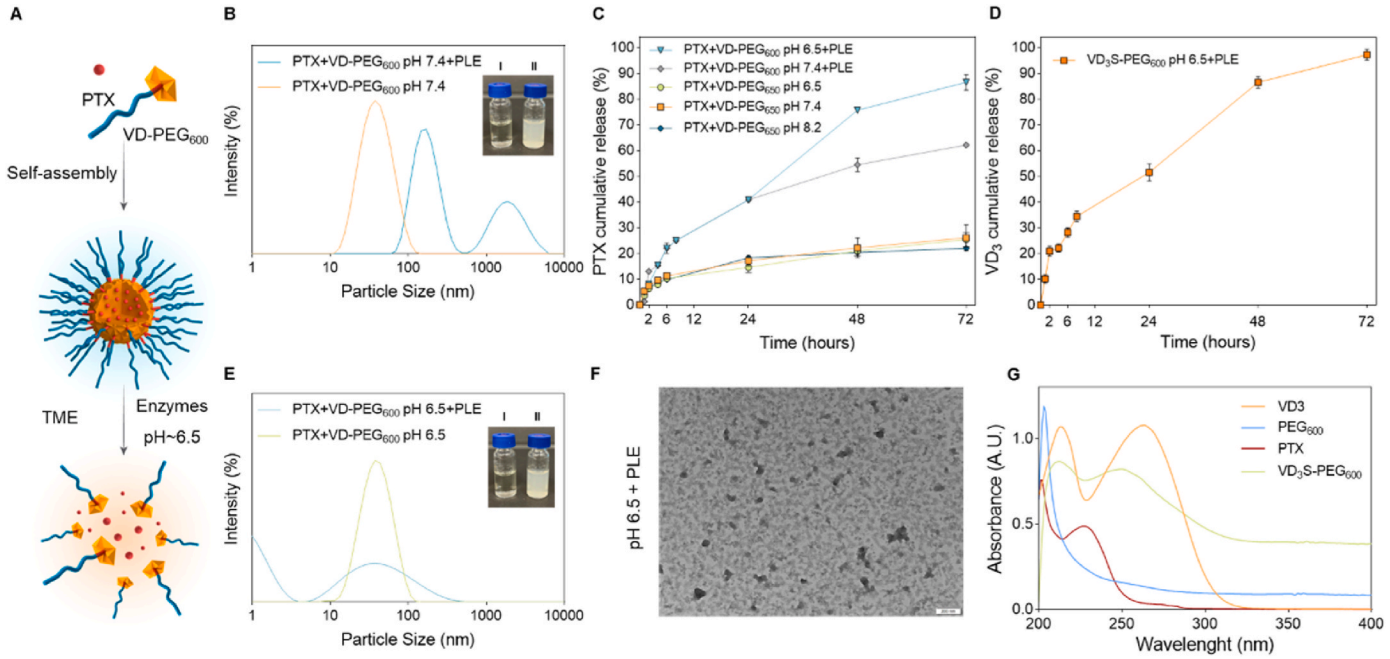

Fig. 5. Enzyme responsiveness behavior of PTX+VD_3S-PEG micelles. **(A)** Scheme of the preparation and release mechanism of the enzyme-responsive PTX + VD_3S-PEG_{600} micelles. **(B)** Particle size of PTX + VD_3S-PEG_{600} measured at pH~7.4 with or without PLE by DLS (n = 3). Inset: Macroscopic appearance of PTX+VD_3S-PEG_{2000} micelles before (I) and after (II) exposure to PLE. **(C)** Release profiles of PTX from VD_3S-PEG_{600} micelles in PBS at pH 6.5, 7.4, and 8.2 with or without PLE, mimicking the pH of the pancreatic TME under normal physiological and normal pancreatic juice conditions (results shown as the mean ± standard deviation, n = 4). **(D)** Release profiles of VD_3 from VD_3S-PEG_{600} micelles in PBS at pH 6.5 with PLE, mimicking the pancreatic TME (results shown as the mean ± standard deviation, n = 4). **(E)** Particle size of PTX+VD_3S-PEG_{600} measured at pH~6.5, with or without PLE, by DLS (n = 3). Inset: Macroscopic appearance of PTX+VD_3S-PEG_{2000} micelles before (I) and after (II) exposure to PLE. **(F)** TEM images of PTX+VD_3S-PEG_{600} at pH~6.5, with PLE (scale bar: 200 nm). **(G)** UV–VIS profile of PTX, VD_3, PEG_{600}, and VD_3S-PEG_{600} in ethanol.

and avoiding off-target effects on healthy cells due to early release of PTX and VD_3. The initial slow hydrolysis of the VD_3S-PEG_{600} conjugate suggested that the presence of the PEG_{600} can initially hinder the enzyme access to the ester bonds. Overall, the results indicate that the ester linker present in the micelles structural unit can remain stable at normal physiological conditions but can be cleaved in the PDAC TME. This validates the PTX release efficiency from micelles and capacity to avoid premature release before entering into PDAC cells, where the ester bond between VD_3 and PEG_{600} can be cleaved by the excessively produced and secreted intracellular esterase.

3.7. Assessment of cellular uptake by confocal microscopy in 2D cell culture models

Cell internalization of VD_3S-PEG_{600} micelles loaded with fluorescent NR, a hydrophobic drug model, was qualitatively studied in BxPC-3 cells using CLSM. Cells were incubated with NR-labelled micelles for 1, 4, and 24 h. After 1 h of incubation, a red fluorescence signal from the encapsulated NR was observed on the cell surface (Fig. S30). Accordingly, NR-labelled micelles were mostly observed within punctate structures associated with the cell surface. After 4 h of incubation, the BxPC-3 cells showed red fluorescence between the cytoplasm (green channel) and the nucleus of BxPC-3 cells (blue channel), revealing that the VD_3S-PEG_{600} micelles were rapidly internalized (Fig. 5B). At 24 h, the morphology of BxPC-3 cells was completely modified due to marked cell death compared with the negative control. After internalization, the ester-bound linkage between VD_3 and PEG can be cleaved by the activity of intracellular catalytic enzymes (esterases) overexpressed in PDAC cells. NR was released rapidly from the VD_3S-PEG_{600} micelles to the cytoplasm and subsequently diffused into the nucleus. Therefore, VD_3S-PEG_{600} micelles demonstrated the ability to encapsulate different highly hydrophobic molecules and favor their transport across the cancer cell membrane of BxPC-3 cells.

3.8. In vitro cytotoxicity of paclitaxel-loaded micelles in 2D and 3D human cell culture models

PDAC is considered one of the most aggressive malignancies owing to its unique TME surrounded by dense and desmoplastic stroma, which consists of approximately 80 % of the tumor mass [3,67]. The desmoplastic stroma is composed of dense collagen-rich ECM that plays an active role in the progression (e.g., migration and invasion) and therapeutic resistance of PDAC [72]. Conventional 2D cell cultures and animal models are the basic approaches currently adopted in PDAC research. However, 2D cell culture models exhibit limitations when attempting to accurately mimic the key hallmarks of the PDAC TME. Indeed, cells growing in 2D monolayers cannot recreate the complexity of the TME and differ in their biological features from cancer cells within the *in vivo* scenario, presenting a less malignant phenotype. To overcome these constraints, *in vitro* 3D cancer models are being developed to more accurately mimic the biological and biochemical diversity of the PDAC TME, to fulfill the *in vitro/in vivo* correlation gap, and ultimately to implement a reduction in laboratory animal research in accordance with 3R's guiding principles (Replacement, Reduction, and Refinement). Among the different tested 3D models, the encapsulation of cells within ECM-mimetic hydrogels has been widely studied as a promising scaffold-based platform for screening possible anticancer treatments [73–75]. These hydrogels for *in vitro* tumor modeling consist of a 3D network of cross-linked materials (i.e., natural or synthetic materials) that swell in an aqueous solution, resembling the bioactivity, viscoelasticity, and mechanical properties of the native ECM, which negatively affects the efficacy of treatments. For instance, Col I is a natural protein extensively found in the ECM of PDAC that can self-assemble into fiber-forming biocompatible hydrogels. Their 3D spatial arrangement presents the potential to establish a biological barrier to nanoplatforms and, thus, allows for an efficient study of their capacity for tumor penetration and delivery of the therapeutic payload. In this study, BxPC-3 cells were encapsulated into Col I-based hydrogels to construct a robust, easy to use, and reproducible 3D model of PDAC. Col I-based hydrogels were obtained by neutralizing the pH of the acidic Col I solution and incubating at 37 ± 2 °C, a crosslinking mechanism that was highly compatible with cell encapsulation (Fig. 6A). The cytotoxicity of free PTX, free VD_3, blank VD_3S-PEG_{600} micelles, and PTX+VD_3S-PEG_{600} micelles was evaluated in both 2D and 3D PDAC culture models using the standard Alamar Blue assay.

Considering that VD_3 may plays a critical role in various cellular processes (i.e., cellular proliferation, cell cycle, cell apoptosis, and angiogenesis), the synergistic effect of VD_3 and PTX on cell cytotoxicity was first investigated in 2D cell culture models (Fig. 6G). In BxPC-3 cells, PTX+VD_3S-PEG_{600} micelles showed a strong cytotoxic effect with lower IC_{50} values than free PTX, free VD_3, and blank VD_3S-PEG_{600} micelles (Table S7). Moreover, both free VD_3 and blank VD_3S-PEG_{600} micelles exhibited improved cytotoxicity compared with free PTX and Abraxane® at high concentrations (10 and 100 μM). The CI value of PTX and VD_3 in PTX+VD_3S-PEG_{600} micelles was 0.86 (CI < 1), indicating a synergistic therapeutic effect of the concomitant administration of PTX and VD_3 formulated as PTX+VD_3-PEG_{600} micelles (Table S7). However, the cytotoxicity of PTX+VD_3S-PEG_{600} micelles in 2D cell culture models only provides a general overview of the response of cancer cells to treatment, since these models are less predictive of the potential *in vivo* response compared to their 3D counterparts. On this basis, it is expected that enzyme-responsive PTX+VD_3S-PEG_{600} micelles can significantly benefit from 3D *in vitro* preclinical models, which better replicate the physiological TME configurations than 2D models, to evaluate the proper (temporal and spatial) delivery of PTX to its target site. Hence, further investigations were performed on 3D cell-laden Col I hydrogels (Fig. S31), which were incubated with free PTX, free VD_3D, blank micelles, and PTX+VD_3S-PEG_{600} micelles for 72 h. In these models, free VD_3, blank VD_3S-PEG_{600} micelles, and PTX+VD_3S-PEG_{600} micelles showed significant growth inhibition of BxPC-3 cells encapsulated in the Col I hydrogels compared to free PTX (Fig. 6H), especially at high PTX concentrations (10 μM and 100 μM). These results were corroborated by the live/dead assay in 3D PDAC culture models, which is a commonly used method for live/dead cell discrimination. Fig. 6D presents the results of the live/dead assay using calcein-AM and ethidium homodimer, in which living cells present a green fluorescence signal by the intracellular enzymatic hydrolysis of calcein AM and dead cells present a red fluorescence signal by the intercalation of ethidium homodimer into DNA after loss of plasma membrane integrity. Free VD_3, blank micelles and PTX+VD_3S-PEG_{600} micelles evidently induced the death of BxPC-3 cells compared to free PTX. The enhanced cytotoxic efficacy of PTX+VD_3S-PEG_{600} micelles could result from the intrinsic anticancer efficacy of VD_3 combined with the faster release of PTX from VD_3S-PEG_{600} micelles triggered by the high esterase level. Upon exposure to the enzyme 25-hydroxyvitamin-1-a-hydroxylase [1a(OH)ase], which is highly expressed in PDAC tissues [76], VD_3 is converted to its biologically active metabolite, calcitriol, which presents a well-documented antitumor activity in both *in vitro* and *in vivo* models [77]. Overall, these observations suggest that simultaneous administration of PTX and VD_3 might result in a synergetic effect with enhanced anticancer efficacy towards PDAC.

3.9. Hemolytic effect

One concern for parenteral administration of micellar formulations is whether the interaction of amphiphilic structural units with erythrocytes affects their cell membrane integrity. This interaction can lead to hemolysis, which refers to the release of intracellular hemoglobin from erythrocytes, either by destruction or *via* a partially damaged but intact cell membrane. *In vivo* hemolysis can lead to anemia, jaundice, and other pathological conditions that may become life-threatening. In addition, extracellular hemoglobin is toxic and may affect vascular, myocardial,

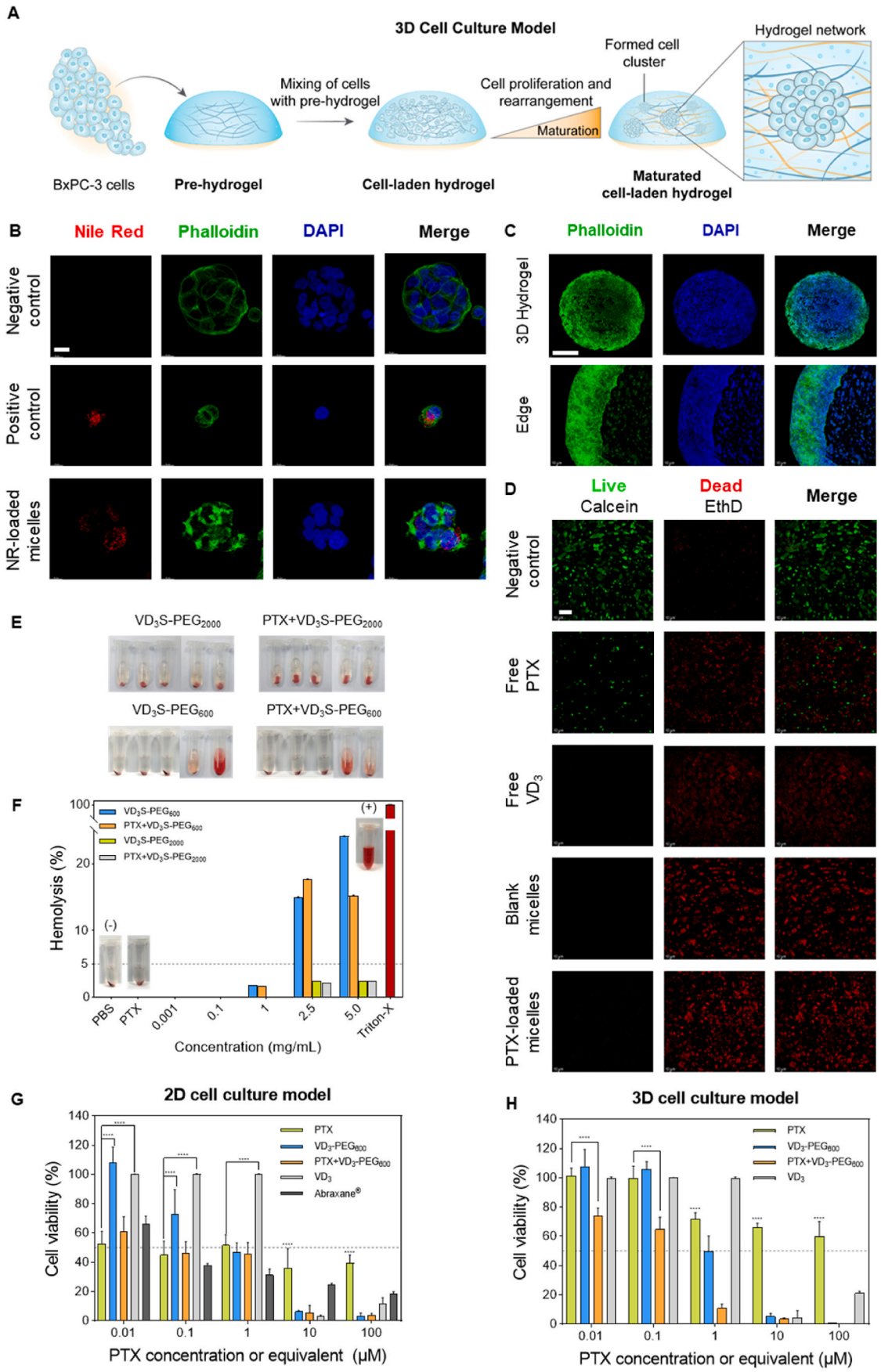

(caption on next page)

Fig. 6. *In vitro* synergistic cytotoxicity of PTX+VD_3S-PEG in 2D and 3D cell culture models. **(A)** Outline of the preparation method of the 3D cell culture model, starting with mixing BxPC-3 cells with a pre-gel based on Col I, followed by cell proliferation and rearrangement (maturation). The mature cell-laden Col I-based hydrogel culture might include cell clusters of rearranged cells, while the original hydrogel network remains (square panel). **(B)** Representative CLSM images (63x) of BxPC-3 cells incubated with NR-loaded VD_3S-PEG_{600} micelles for 4 h (scale bar: 10 μm). CLSM images were taken of the cell cytoskeleton (filamentous actin) stained with Alexa Fluor 488 phalloidin (column 2, green), cell nuclei stained with DAPI (column 3, blue), and merged images of both channels (column 4). Complete RPMI cell culture medium and free NR (0.5 μg/mL) were used as the negative and positive controls, respectively. **(C)** Representative CSLM images of 3D cell-laden Col I-based hydrogels at day 3 post-seeding (i.e., 3 days after BxPC-3 addition during Col I-based hydrogel preparation (Scale bar: 10 μm). **(D)** Live/dead staining of BxPC-3 cells within Col I-based hydrogels after 72h of incubation with PTX+VD_3S-PEG_{600} micelles (green, live cells; red, dead cells; scale bar: 100 μm). **(E)** Macroscopic appearance and **(F)** hemolysis percentage produced by free PTX (1 mg/mL), blank, and PTX+VD_3S-PEG micelles after 1 h of incubation at 37 °C under gentle agitation. PBS and 4 % Triton X-100 aqueous solution were used as the negative (−) control (0 % hemolysis) and positive (+) control (100 % hemolysis), respectively. **(G)** Percentage of BxPC-3 cell viability as a function of free PTX, free VD_3, blank VD_3S-PEG_{600} micelles, PTX+VD_3S-PEG_{600} micelles, and Abraxane® at an incubation time of 72 h (2D models). The equivalent concentration of free VD_3 was estimated from the amount of VD_3 present in 50 mg of the VD_3S-PEG conjugate used to prepare PTX+VD_3S-PEG_{600} micelles at a mass ratio of 50:1 (w/w). **(H)** Percentage of BxPC-3 cell viability after incubating the cell-laden hydrogels with different concentrations of free PTX, free VD_3, blank VD_3S-PEG_{600} micelles, and PTX+VD_3S-PEG_{600} micelles for 72 h (3D models). Results are expressed as mean ± standard deviation, *$p < 0.05$, **$p < 0.005$, ***$p < 0.001$, and ****$p < 0.0001$. (For interpretation of the references to color in this figure legend, the reader is referred to the Web version of this article.)

renal, and central nervous system functions. Therefore, the amount of extracellular hemoglobin should be minimal to ensure the absence of toxicity in the administered micellar formulations. In this context, the hemocompatibility of PTX+VD_3S-PEG_{600} micelles and blank VD_3S-PEG_{600} micelles at high VD_3S-PEG concentrations (2.5 and 5 mg/mL) was estimated by determining the hemolysis percentage. As shown in Fig. 6F, the hemolysis percentage was <5 % for all tested blank VD_3S-PEG_{2000} and PTX+VD_3S-PEG_{2000} micelles, whereas the hemolysis percentage was >10 % for VD_3S-PEG_{600} micelles and PTX+VD_3S-PEG_{600} micelles when their concentration was above 2.5 mg/mL. The obtained results indicate that micelles composed of VD_3S-PEG_{600} are non-hemocompatible at high concentrations, which could be due to more intense: (i) insertion of the conjugate into the membrane, and (ii) membrane-disturbing action of the conjugate, compared to the conjugate with the longer PEG [78]. In contrast, blank VD_3S-PEG_{600} micelles and PTX+VD_3S-PEG_{600} micelles at low concentrations (up to 1.0 mg/mL) exhibited negligible hemolytic activity (Fig. 6E and F). These results were corroborated by the HET-CAM assay, since no hemorrhage, clotting, vascular lysis, or vessel bleeding were observed when VD_3S-PEG_{600} and PTX+VD_3S-PEG_{600} micelles contacted the CAM (Fig. S31), with similar results to those observed for the negative control (0.9 % NaCl).

3.10. *In ovo* antitumor effect of paclitaxel-loaded micelles

The transition from 2D to 3D cell culture models plays a pivotal role in improving biomimetic tumor models. However, 3D cell culture models are static and fail to replicate the dynamic biological signals within the TME due to the absence of vascularization [79]. Therefore, preclinical cancer research requires more sophisticated models for the development and translation of efficient and safe therapeutic strategies to clinical practice. The *in ovo* CAM assay has attracted a lot of attention as an alternative for the *in vivo* murine model in preclinical oncological research of several types of cancer, including PDAC [80]. Tumor-grafted CAM models are simple and cost-effective biological models that mimic the dynamic roles of TME and cancer physiopathology. The highly vascularized CAM connected to the embryo through a continuous circulatory system and the absence of immune system until ED17 provide an ideal environment for efficient tumor growth during a short period of time [80,81]. Moreover, the *in ovo* CAM assay usually does not require permission or approval from ethics committees, since the chick embryo does not develop pain perception until ED 17. Accordingly, the *in ovo* CAM assay allows the straightforward evaluation of anticancer activity of nanoformulations in agreement with the 3Rs principle, in line with Directive 2010/63/EU and the FDA Modernization Act 3.0 [45].

In the present work, the *in ovo* CAM assay was performed to investigate the ability of PTX+VD_3S-PEG_{600} micelles to suppress the growth of BxPC-3 primary tumor in comparison to free PTX, VD_3, VD_3S-PEG_{600} micelles, and Abraxane®. A high initial concentration of BxPC-3 cells (2×10^6) in Matrigel was properly grafted on the CAM at the ED6 to promote the growth of a macroscopically visible tumor, which facilitated the further analyses. At ED10 preliminary macroscopic visual analysis revealed a correct tumor grafting and formation, similar to previously described procedures [80,82]. At this time, *in ovo* BxPC-3 tumors were treated with PTX, VD_3, VD_3S-PEG_{600} micelles, and Abraxane® (equivalent concentration of PTX was 100 μM). After four days (ED14), all the embryos were viable and growing correctly, showing no sign of toxicity and hemolysis. However, the tumors observed from the exposed surface of the CAM presented a monolayer appearance, rather than a 3D architecture (Fig. S32). Therefore, tumors and distal CAM were collected to confirm the development of a 3D primary tumor on the inner surface of the CAM. By applying this method, it was possible to directly observe a microtumor on the inner surface of the CAM, where blood vessels were strongly concentrated around the tumor (Fig. 7B). Considering that cytostatic agents are known to reduce the extent of the overall vascular density of tumors [80], images of the CAM were taken using a stereomicroscope to determine the number of intratumoral and peritumoral vessels and evaluate the effect of all applied treatments on the inhibition of tumor angiogenesis. The treatment with PTX+VD_3S-PEG_{600} micelles was the most successful in diminishing the number of intratumoral microvessels; this was the only formulation able to induce significant changes in tumor angiogenesis compared to the control group (Fig. 7E). Upon termination, tumors were excised from the CAM and the assessment of the BxPC-3 primary tumor growth was performed by weight measurements (Fig. 7D). PTX+VD_3S-PEG_{600} micelles demonstrated a significant antitumoral activity compared to untreated tumors and free PTX (Fig. 7C). The results were consistent with the evaluation of tumor angiogenesis and, in both cases, PTX-VD_3S-PEG_{600} micelles outperformed the clinical gold standard Abraxane® at equivalent doses. The enhanced inhibitory effect on the tumor size and angiogenesis by PTX-VD_3S-PEG_{600} micelles may result from the synergistic anticancer effect of PTX with VD_3 against human PDAC cells (BxPC-3 cells), as shown *in vitro* (Fig. 6). Another important feature is the particle size of PTX+VD_3S-PEG_{600} micelles (*ca.* 46 nm), since nanoformulations with 50 nm or less have demonstrated the capacity to successfully penetrate poorly permeable hypovascular tumors like PDAC [19,82,83].

4. Conclusions and future work

In summary, multifunctional and microenvironmental enzyme-sensitive micelles were developed for the controlled release of the chemotherapeutic drug PTX for PDAC treatment. Two enzyme-responsive VD_3S-PEG conjugates with varying molecular weights of PEG (PEG_{600} *vs.* PEG_{2000}) were developed to prepare micelles using the solvent evaporation method. PTX was efficiently encapsulated inside the core of the prepared VD_3S-PEG micelles (PTX + VD_3S-PEG_{600} and PTX+VD_3S-PEG_{2000}) *via* hydrophobic interactions, protecting it from

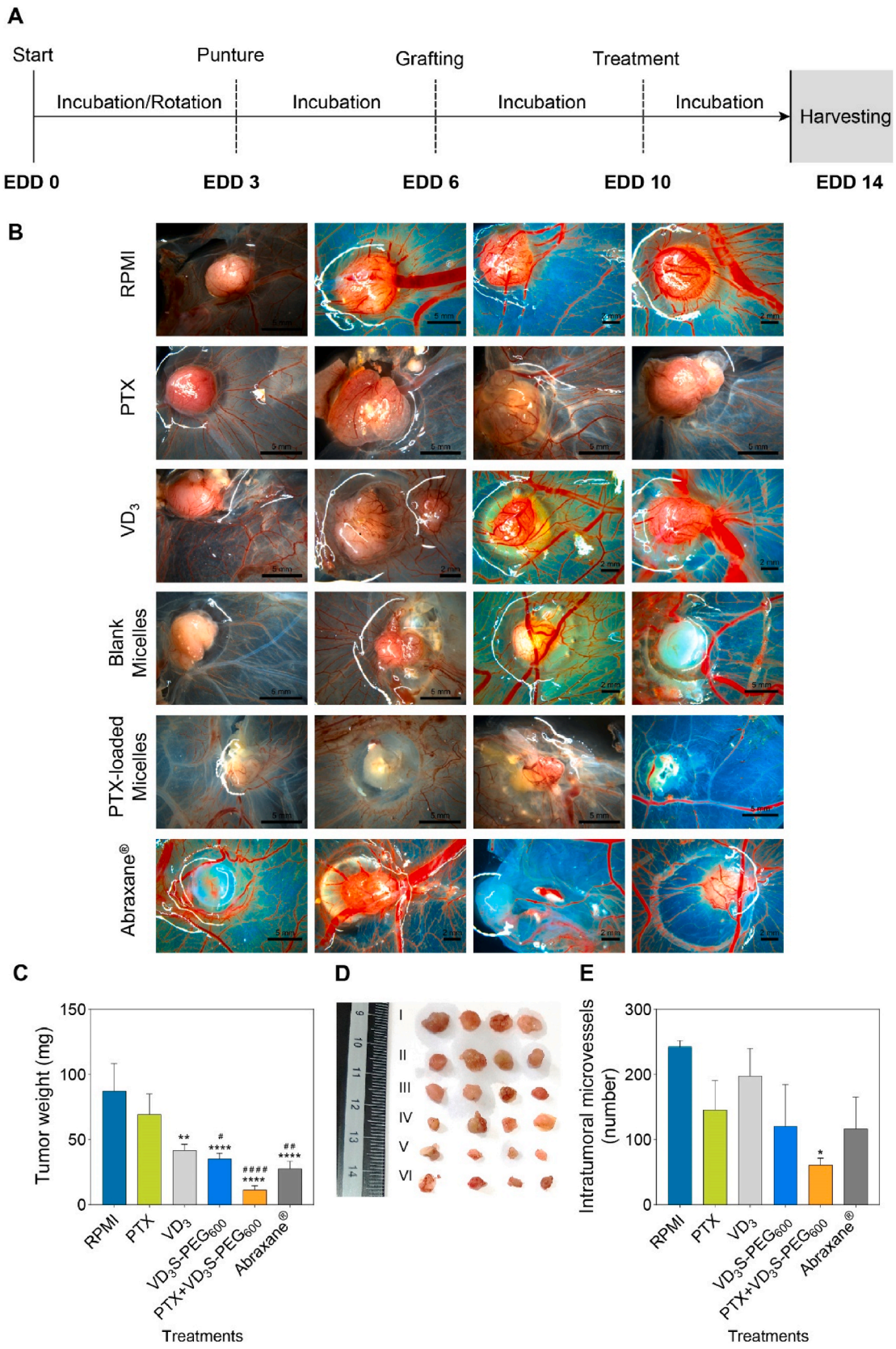

Fig. 7. *In ovo* CAM assay. **(A)** Experimental outline**. (B)** Photographs of the CAM grafted with BxPC-3 cells (upon experiment termination on ED 14) after treatment with free PTX, free VD_3, VD_3S-PEG_{600} micelles, PTX+VD_3S-PEG_{600} micelles, and Abraxane® (equivalent concentration of PTX was 100 μM). **(C)** Average tumor weights after treatment. (**D**) Represent images of excised tumors without treatment (I) and after treatment with free PTX (II), free VD_3 (III), VD_3S-PEG_{600} micelles (IV), PTX+VD_3S-PEG_{600} micelles (V), and Abraxane® (VI). **(E)** Number of intratumoral vessels for each treatment. Results are reported as mean ± standard deviation (n = 4). Asterisk (*) was used to compare the antitumoral activity with the untreated group and number sign (#) was use was used to compare the antitumoral activity with free PTX.

premature leakage under physiological conditions. All micellar formulations were optimized with respect to the VD_3S-PEG conjugate/PTX mass ratio to yield sub-100 nm micelles with a spherical morphology, minimal batch-to-batch variation, monomodal particle size distribution, and high encapsulation efficiency. More importantly, the PTX+VD_3S-PEG_{600} conjugate was significantly more effective than the PTX+VD-PEG_{2000} conjugate in forming stable micelles and mediating controlled release of PTX. Consequently, PTX+VD_3S-PEG_{600} micelles were selected as the most suitable formulations to further evaluate enzyme responsiveness and *in vitro* anticancer activity. With the help of the ester bond linkage between VD and PEG_{600}, PTX+VD_3S-PEG_{600} micelles were capable of selectively disassembling when the pH varied from 7.4 to 6.5 and in the presence of elevated intracellular esterase content featured by the inner part of the TME, leading to PTX release. *In vitro* studies with human PDAC BxPC-3 cells clearly demonstrated efficient cellular internalization of PTX+VD_3S-PEG_{600} micelles. After successful internalization by BxPC-3 cells, the structure of PTX+VD_3S-PEG_{600} micelles was disrupted, allowing rapid intracellular co-delivery of VD_3 and PTX, which synergistically exerted a significant anticancer effect compared to PTX alone. In a more complex 3D cell-laden hydrogel, PTX+VD_3S-PEG_{600} micelles exhibited excellent anticancer activity. This type of 3D cell culture model is currently validated as a strategy to not only mimic the TME *in vitro* but also to reduce the gap between easy-to-use but poorly representative 2D cell culture models. Finally, as an alternative to *in vivo* studies, an *in ovo* CAM assay was performed, where PTX+VD_3S-PEG_{600} micelles showed strong capacity to suppress tumor growth compared to the clinical approved Abraxane®. Collectively, these results demonstrate the interest of VD_3S-PEG as a multifunctional building block, and the remarkable anticancer activity of VD_3 provides a new idea for a potential combination treatment against PDAC and opens a new window for improving the application of PTX in PDAC. However, research on VD_3-based micellar systems is still in its preliminary stages, with many areas to be explored before clinical translation, such as the exploration of the encapsulation of different bioactive molecules and evaluation of anticancer activity in 3D PDAC multicellular models, followed by *in vivo* studies.

CRediT authorship contribution statement

Diana Peixoto: Writing – review & editing, Writing – original draft, Visualization, Validation, Software, Methodology, Investigation, Formal analysis, Data curation, Conceptualization. **João M. Ravasco:** Writing – review & editing, Writing – original draft, Visualization, Supervision, Software, Methodology, Investigation. **Barbara Blanco-Fernandez:** Writing – review & editing, Writing – original draft, Visualization, Supervision, Software, Methodology, Investigation. **Francisco Veiga:** Writing – review & editing, Supervision, Funding acquisition, Conceptualization. **Angel Concheiro:** Writing – review & editing, Writing – original draft, Supervision, Resources, Project administration, Funding acquisition, Conceptualization. **João Conde:** Writing – review & editing, Writing – original draft, Validation, Supervision, Resources, Project administration, Methodology, Investigation, Funding acquisition, Conceptualization. **Ana Cláudia Paiva-Santos:** Writing – review & editing, Writing – original draft, Validation, Supervision, Resources, Project administration, Methodology, Investigation, Funding acquisition, Conceptualization. **Carmen Alvarez-Lorenzo:** Writing – review & editing, Writing – original draft, Visualization, Validation, Supervision, Software, Resources, Project administration, Methodology, Investigation, Funding acquisition, Formal analysis, Data curation, Conceptualization.

Funding

The work was supported by MCIN/AEI/10.13039/501100011033 [PID2023-150422OB-I00] Spain, FEDER and Xunta de Galicia [ED431C 2024/09]. The work was also supported by the Ph.D. research grant 2021.05914.BD from the Fundação para a Ciência e Tecnologia (FCT, Portugal). B.B.-F. is grateful to the Spanish AEI for the Ramón y Cajal fellowship (no. RYC2022-037421-I).

Declaration of competing interest

The authors declare the following financial interests/personal relationships which may be considered as potential competing interests: Diana Peixoto reports financial support was provided by Fundação para a Ciência e Tecnologia. Barbara Blanco-Fernandez reports financial support was provided by Agencia Estatal de Investigación (AEI). Carmen Alvarez-Lorenzo reports a relationship with Elsevier Inc- International Journal of Pharmaceutics that includes: board membership. If there are other authors, they declare that they have no known competing financial interests or personal relationships that could have appeared to influence the work reported in this paper.

Acknowledgements

The authors acknowledge the crucial assistance of Ignacio Insua-Lopez with the characterization of cholecalciferol succinate-polyethylene glycol conjugates; Iago Gonzalez-Prada with HPLC analysis, hemolysis test, contact angle experiments, and *in ovo* assay; Maria Vivero-López with the preparation of micelles and HPLC analysis; Nicola Filippo Virzi with computational modeling; and Patricia Diaz-Rodriguez with *in ovo* assay.

Abbreviations

2D	Two-Dimensional
3D	Three-Dimensional
BCS	Biopharmaceutical Classification System
CAF	Cancer-Associated Fibroblast
CLSM	Confocal Laser Scanning Microscopy
CMC	Critical Micellar Concentration
Col I	Collagen I
DL	Drug Loading
DLS	Dynamic Light Scattering
ECM	Extracellular Matrix
EE	Encapsulation Efficiency
ELS	Electrophoretic Light Scattering
EMA	European Medicines Agency
EPR	Enhanced Permeability and Retention
FBS	Fetal Bovine Serum
FDA	Food and Drug Administration
HPLC	High-Performance Liquid Chromatography
IC_{50}	Half-Maximal Inhibitory Concentration
ICH	International Council for Harmonisation
LOD	Limits of Detection
LOQ	Limits of Quantification
MDR	Multiple Drug Resistance
MRP1	Multidrug Resistance-Associated Protein 1
MW	Molecular Weight
PBS	Phosphate-Buffered Saline
PDAC	Pancreatic Ductal Adenocarcinoma
PDI	Polydispersity Index
PEG	Polyethylene Glycol
P-gp-P	Glycoprotein
PLE	Porcine Liver Esterase
PTX	Paclitaxel
TEM	Transmission Electron Microscope
TME	Tumor Microenvironment
UV	Ultraviolet
VD	Vitamin D
ZP	Zeta Potential

Appendix A. Supplementary data

Supplementary data to this article can be found online at https://doi.org/10.1016/j.mtbio.2025.101555.

Data availability

Data will be made available on request.

References

[1] C.J. Halbrook, C.A. Lyssiotis, M. Pasca di Magliano, A. Maitra, Pancreatic cancer: advances and challenges, Cell 186 (2023) 1729–1754, https://doi.org/10.1016/j.cell.2023.02.014.

[2] R.L. Siegel, K.D. Miller, H.E. Fuchs, A. Jemal, Cancer statistics, CA A Cancer J. Clin. 72 (2022) 7–33, https://doi.org/10.3322/caac.21708, 2022.

[3] W.J. Ho, E.M. Jaffee, L. Zheng, The tumour microenvironment in pancreatic cancer — clinical challenges and opportunities, Nat. Rev. Clin. Oncol. 17 (2020) 527–540, https://doi.org/10.1038/s41571-020-0363-5.

[4] Z.I. Hu, E.M. O'Reilly, Therapeutic developments in pancreatic cancer, Nat. Rev. Gastroenterol. Hepatol. 21 (2024) 7–24, https://doi.org/10.1038/s41575-023-00840-w.

[5] J.P. Neoptolemos, J. Kleeff, P. Michl, E. Costello, W. Greenhalf, i D.H. Palmer, Therapeutic developments in pancreatic cancer: current and future perspectives, Nat. Rev. Gastroenterol. Hepatol. 15 (2018) 333–348, https://doi.org/10.1038/s41575-018-0005-x.

[6] T. Conroy, et al., FOLFIRINOX versus gemcitabine for metastatic pancreatic cancer, N. Engl. J. Med. 364 (2011) 1817–1825, https://doi.org/10.1056/nejmoa1011923.

[7] L.B. Saltz, P.B. Bach, Albumin-bound paclitaxel plus gemcitabine in pancreatic cancer, N. Engl. J. Med. 370 (2014) 478–480, https://doi.org/10.1056/NEJMc1314761.

[8] X. Chen, H.J. Zeh, R. Kang, G. Kroemer, D. Tang, Cell death in pancreatic cancer: from pathogenesis to therapy, Nat. Rev. Gastroenterol. Hepatol. 18 (2021) 804–823, https://doi.org/10.1038/s41575-021-00486-6.

[9] H. Huang, et al., Nanoenabled reversal of Ido1-mediated immunosuppression synergizes with immunogenic chemotherapy for improved cancer therapy, Nano Lett. 19 (2019) 5356–5365, https://doi.org/10.1021/acs.nanolett.9b01807.

[10] O. Yusuf, et al., Design and development of d-α-tocopheryl polyethylene glycol succinate-block-poly(ε-caprolactone) (TPGS−b−PCL) nanocarriers for solubilization and controlled release of paclitaxel, Molecules 26 (2021) 2690, https://doi.org/10.3390/molecules26092690.

[11] X. Zhao, et al., Inducing enhanced immunogenic cell death with nanocarrier-based drug delivery systems for pancreatic cancer therapy, Biomaterials 102 (2016) 187–197, https://doi.org/10.1016/j.biomaterials.2016.06.032.

[12] F. Kratz, Albumin as a drug carrier: design of prodrugs, drug conjugates and nanoparticles, J. Contr. Release 132 (2008) 171–183, https://doi.org/10.1016/j.jconrel.2008.05.010.

[13] Z. He, et al., A high capacity polymeric micelle of paclitaxel: implication of high dose drug therapy to safety and in vivo anti-cancer activity, Biomaterials 101 (2016) 296–309, https://doi.org/10.1016/j.biomaterials.2016.06.002.

[14] Y. Min, J.M. Caster, M.J. Eblan, A.Z. Wang, Clinical translation of nanomedicine, Chem. Rev. 115 (2015) 11147–11190, https://doi.org/10.1021/acs.chemrev.5b00116.

[15] N. Hirakawa, et al., Reduction-responsive and multidrug deliverable albumin nanoparticles: an antitumor drug to Abraxane against human pancreatic tumor-bearing mice, ACS Appl. Bio Mater. 4 (2021) 4302–4309, https://doi.org/10.1021/acsabm.1c00110.

[16] J. Riedel, et al., Paclitaxel and curcumin co-loaded mixed micelles: improving in vitro efficacy and reducing toxicity against Abraxane®, J. Drug Deliv. Sci. Technol. 62 (2021) 102343 https://doi.org/10.1016/j.jddst.2021.102343.

[17] J. Chen, et al., Enzyme and reduction dual-responsive peptide micelles as nanocarriers for smart drug delivery, ACS Appl. Nano Mater. 6 (2023) 16179–16188, https://doi.org/10.1021/acsanm.3c02059.

[18] N. Ying, et al., Nano delivery system for paclitaxel: recent advances in cancer theranostics, Colloids Surf. B Biointerfaces 228 (2023) 113419, https://doi.org/10.1016/j.colsurfb.2023.113419.

[19] H. Cabral, et al., Accumulation of sub-100 nm polymeric micelles in poorly permeable tumours depends on size, Nat. Nanotechnol. 6 (2011) 815–823, https://doi.org/10.1038/nnano.2011.166.

[20] J. Gong, M. Chen, Y. Zheng, S. Wang, Y. Wang, Polymeric micelles drug delivery system in oncology, J. Contr. Release 159 (2012) 312–323, https://doi.org/10.1016/j.jconrel.2011.12.012.

[21] M.J. Mitchell, M.M. Billingsley, R.M. Haley, M.E. Wechsler, N.A. Peppas, R. Langer, Engineering precision nanoparticles for drug delivery, Nat. Rev. Drug Discov. 20 (2021) 101–124, https://doi.org/10.1038/s41573-020-0090-8.

[22] J. Sun, et al., Triple drugs co-delivered by a small gemcitabine-based carrier for pancreatic cancer immunochemotherapy, Acta Biomater. 106 (2020) 289–300, https://doi.org/10.1016/j.actbio.2020.01.039.

[23] J. Sun, et al., A prodrug micellar carrier assembled from polymers with pendant farnesyl thiosalicylic acid moieties for improved delivery of paclitaxel, Acta Biomater. 43 (2016) 282–291, https://doi.org/10.1016/j.actbio.2016.07.014.

[24] H. Cabral, K. Miyata, K. Osada, K. Kataoka, Block copolymer micelles in nanomedicine applications, Chem. Rev. 118 (2018) 6844–6892, https://doi.org/10.1021/acs.chemrev.8b00199.

[25] X. Chen, et al., Codelivery nanosystem targeting the deep microenvironment of pancreatic cancer, Nano Lett. 19 (2019) 3527–3534, https://doi.org/10.1021/acs.nanolett.9b00374.

[26] B. Sui, C. Cheng, S. Shi, M. Wang, P. Xu, Esterase-activatable and glutathione-responsive triptolide nano-prodrug for the eradication of pancreatic cancer, Adv. NanoBiomed Res. 1 (2021) 2100040, https://doi.org/10.1002/anbr.202100040.

[27] D. Feldman, A.V. Krishnan, S. Swami, E. Giovannucci, B.J. Feldman, The role of vitamin D in reducing cancer risk and progression, Nat. Rev. Cancer 14 (2014) 342–357, https://doi.org/10.1038/nrc3691.

[28] K.K. Deeb, D.L. Trump, C.S. Johnson, Vitamin D signalling pathways in cancer: potential for anticancer therapeutics, Nat. Rev. Cancer 7 (2007) 684–700, https://doi.org/10.1038/nrc2196.

[29] S.G. Barreto, R.E. Neale, Vitamin D and pancreatic cancer, Cancer Lett. 368 (2015) 1–6, https://doi.org/10.1016/j.canlet.2015.06.030.

[30] M. Yan, H. Nuriding, Reversal effect of vitamin D on different multidrug-resistant cells, Genet. Mol. Res. 13 (2014) 6239–6247, https://doi.org/10.4238/2014.August.15.6.

[31] C. Chang, P.M. Bahadduri, J.E. Polli, P.W. Swaan, S. Ekins, Rapid identification of P-glycoprotein substrates and inhibitors, Drug Metab. Dispos. 34 (2006) 1976–1984, https://doi.org/10.1124/dmd.106.012351.

[32] K.W. Tan, A. Sampson, B. Osa-Andrews, S.H. Iram, Calcitriol and calcipotriol modulate transport activity of ABC transporters and exhibit selective cytotoxicity in MRP1-overexpressing cells, Drug Metab. Dispos. 46 (2018) 1856–1866, https://doi.org/10.1124/dmd.118.081612.

[33] V. Bhattacharjee, Y. Zhou, T.J. Yen, A synthetic lethal screen identifies the vitamin D receptor as a novel gemcitabine sensitizer in pancreatic cancer cells, Cell Cycle 13 (2014) 3839–3856, https://doi.org/10.4161/15384101.2014.967070.

[34] F. Innocenti, et al., The Vitamin D receptor gene as a determinant of survival in pancreatic cancer patients: genomic analysis and experimental validation, PLoS One 13 (2018) 1–14, https://doi.org/10.1371/journal.pone.0202272.

[35] M.H. Sherman, et al., Vitamin D receptor-mediated stromal reprogramming suppresses pancreatitis and enhances pancreatic cancer therapy, Cell 159 (2014) 80–93, https://doi.org/10.1016/j.cell.2014.08.007.

[36] L. Gorchs, et al., The vitamin D analogue calcipotriol promotes an anti-tumorigenic phenotype of human pancreatic CAFs but reduces T cell mediated immunity, Sci. Rep. 10 (2020) 1–15, https://doi.org/10.1038/s41598-020-74368-3.

[37] M. Cutolo, V. Smith, S. Paolino, E. Gotelli, Involvement of the secosteroid vitamin D in autoimmune rheumatic diseases and COVID-19, Nat. Rev. Rheumatol. 19 (2023) 265–287, https://doi.org/10.1038/s41584-023-00944-2.

[38] H.Z. Zhao, E.C. Tan, L.Y.L. Yung, Potential use of cholecalciferol polyethylene glycol succinate as a novel pharmaceutical additive, J. Biomed. Mater. Res., Part A 84 (2008) 954–964, https://doi.org/10.1002/jbm.a.31402.

[39] S. Kutlehria, et al., Cholecalciferol-PEG conjugate based nanomicelles of doxorubicin for treatment of triple-negative breast cancer, AAPS PharmSciTech 19 (2018) 792–802, https://doi.org/10.1208/s12249-017-0885-z.

[40] N. Gao, Y. Fu, H. Gong, H. Liu, W. Li, Hyaluronic acid and cholecalciferol conjugate based nanomicelles: synthesis, characterization, and cytotoxicity against MCF-7 breast cancer cells, Carbohydr. Res. 522 (2022) 108706, https://doi.org/10.1016/j.carres.2022.108706.

[41] S. Patil, S. Gawali, S. Patil, S. Basu, Synthesis, characterization and in vitro evaluation of novel vitamin D3 nanoparticles as a versatile platform for drug delivery in cancer therapy, J. Mater. Chem. B 42 (2013) 5742–5750, https://doi.org/10.1039/c3tb21176b.

[42] S. Palvai, J. Nagraj, N. Mapara, R. Chowdhury, S. Basu, Dual drug loaded vitamin D3 nanoparticle to target drug resistance in cancer, RSC Adv. 4 (2014) 57271–57281, https://doi.org/10.1039/c4ra06475e.

[43] J.J. Han, FDA Modernization Act 2.0 allows for alternatives to animal testing, Artif. Organs 47 (2023) 449–450, https://doi.org/10.1111/aor.14503.

[44] C.D. Logsdon, T. Arumugam, V. Ramachandran, Animal models of gastrointestinal and liver diseases. the difficulty of animal modeling of pancreatic cancer for preclinical evaluation of therapeutics, Am. J. Physiol. Gastrointest. Liver Physiol. 309 (2015) G283–G291, https://doi.org/10.1152/ajpgi.00169.2015.

[45] E. Preis, J. Schulze, B. Gutberlet, S.R. Pinnapireddy, J. Jedelská, U. Bakowsky, The chorioallantoic membrane as a bio-barrier model for the evaluation of nanoscale drug delivery systems for tumour therapy, Adv. Drug Deliv. Rev. 174 (2021) 317–336, https://doi.org/10.1016/j.addr.2021.04.022.

[46] C.J. Van Oss, L. Ju, M.K. Chaudhury, R.J. Good, Estimation of the polar parameters of the surface tension of liquids by contact angle measurements on gels, J. Colloid Interface Sci. 128 (1989) 313–319, https://doi.org/10.1016/0021-9797(89)90345-7.

[47] N. Coudon, et al., Stabilization of all-aqueous droplets by interfacial self-assembly of fatty acids bilayers, J. Colloid Interface Sci. 617 (2022) 257–266, https://doi.org/10.1016/j.jcis.2022.02.138.

[48] M.A. Grimaudo, et al., Poloxamer 407/TPGS mixed micelles as promising carriers for cyclosporine ocular delivery, Mol. Pharm. 15 (2018) 571–584, https://doi.org/10.1021/acs.molpharmaceut.7b00939.

[49] I. Fuentes, et al., Encapsulation of antioxidant gallate derivatives in biocompatible poly(ε-caprolactone)-b-Pluronic-b-poly(ε-caprolactone) micelles, Langmuir 32 (2016) 3331–3339, https://doi.org/10.1021/acs.langmuir.5b04748.

[50] B. Blanco-Fernandez, A. Concheiro, H. Makwana, F. Fernandez-Trillo, C. Alexander, C. Alvarez-Lorenzo, Dually sensitive dextran-based micelles for methotrexate delivery, RSC Adv. 7 (2017) 14448–14460, https://doi.org/10.1039/c7ra00696a.

[51] A. Cambón, et al., Doxorubicin-loaded micelles of reverse poly(butylene oxide)-poly(ethylene oxide)-poly(butylene oxide) block copolymers as efficient ‚active' chemotherapeutic agents, Int. J. Pharm. 445 (2013) 47–57, https://doi.org/10.1016/j.ijpharm.2013.01.056.
[52] A.P. Krawczyk-Santos, R.N. Marreto, A. Concheiro, C. Alvarez-Lorenzo, S. F. Taveira, Poly(pseudo)rotaxanes formed by mixed micelles and α-cyclodextrin enhance terbinafine nail permeation to deeper layers, Int. J. Pharm. X 4 (2022) 100118, https://doi.org/10.1016/j.ijpx.2022.100118.
[53] M. Magalhães, et al., miR-145-loaded micelleplexes as a novel therapeutic strategy to inhibit proliferation and migration of osteosarcoma cells, Eur. J. Pharmaceut. Sci. 123 (2018) 28–42, https://doi.org/10.1016/j.ejps.2018.07.021.
[54] M. Panagi, et al., Polymeric micelles effectively reprogram the tumor microenvironment to potentiate nano-immunotherapy in mouse breast cancer models, Nat. Commun. 13 (2022) 7165, https://doi.org/10.1038/s41467-022-34744-1.
[55] B. Blanco-Fernandez, et al., Elastin-like recombinamer hydrogels as platforms for breast cancer modeling, Biomacromolecules 24 (2023) 4408–4418, https://doi.org/10.1021/acs.biomac.2c01080.
[56] N.M.R. Nakka, et al., Dual drug-loaded tumor-targeted polymeric nanoparticles for enhancing therapeutic response in pancreatic ductal adenocarcinoma, Mater. Today Bio 28 (2024) 101199, https://doi.org/10.1016/j.mtbio.2024.101199.
[57] N. Rajan, J. Habermehl, M.-F. Coté, C.J. Doillon, D. Mantovani, Preparation of ready-to-use, storable and reconstituted type I collagen from rat tail tendon for tissue engineering applications, Nat. Protoc. 1 (2006) 2753–2758, https://doi.org/10.1038/nprot.2006.430.
[58] B. Blanco-Fernandez, et al., Bioprinting decellularized breast tissue for the development of three-dimensional breast cancer models, ACS Appl. Mater. Interfaces 14 (2022) 29467–29482, https://doi.org/10.1021/acsami.2c00920.
[59] N.F. Virzì, et al., Heme oxygenase 1 inhibitor discovery and formulation into nanostructured lipid carriers as potent and selective treatment against triple negative metastatic breast cancer, Int. J. Pharm. 668 (2025) 124997, https://doi.org/10.1016/j.ijpharm.2024.124997.
[60] V. Khare, W. Al Sakarchi, P.N. Gupta, A.D.M. Curtis, C. Hoskins, Synthesis and characterization of TPGS-gemcitabine prodrug micelles for pancreatic cancer therapy, RSC Adv. 6 (2016) 60126–60137, https://doi.org/10.1039/c6ra09347g.
[61] J.O. Naim, C.J. van Oss, The effect of hydrophilicity-hydrophobicity and solubility on the immunogenicity of some natural and synthetic polymers, Immunol. Investig. 21 (1992) 649–662, https://doi.org/10.3109/08820139209069401.
[62] M. Bagheri, et al., Effect of formulation and processing parameters on the size of mPEG-b-p(HPMA-Bz) polymeric micelles, Langmuir 34 (2018) 15495–15506, https://doi.org/10.1021/acs.langmuir.8b03576.
[64] J. Lu, et al., Design and characterization of PEG-derivatized vitamin e as a nanomicellar formulation for delivery of paclitaxel, Mol. Pharm. 10 (2013) 2880–2890, https://doi.org/10.1021/mp300729y.
[66] B.Y. Liu, C. Wu, X.Y. He, R.X. Zhuo, S.X. Cheng, Multi-drug loaded vitamin E-TPGS nanoparticles for synergistic drug delivery to overcome drug resistance in tumor treatment, Sci. Bull. 61 (2016) 552–560, https://doi.org/10.1007/s11434-016-1039-5.
[67] ICH Expert Working Group, ICH harmonised guideline - impurities: guideline for residual solvents Q3C(R8), Int. Counc. Harmon. Tech. Requir. Pharm. Hum. Use April (2021) 1–43.
[68] S. Lv, et al., High drug loading and sub-quantitative loading efficiency of polymeric micelles driven by donor-receptor coordination interactions, J. Am. Chem. Soc. 140 (2018) 1235–1238, https://doi.org/10.1021/jacs.7b12776.
[69] S.C. Owen, D.P.Y. Chan, M.S. Shoichet, Polymeric micelle stability, Nano Today 7 (2012) 53–65, https://doi.org/10.1016/j.nantod.2012.01.002.
[70] A.E. Nel, et al., Understanding biophysicochemical interactions at the nano–bio interface, Nat. Mater. 8 (2009) 543–557, https://doi.org/10.1038/nmat2442.
[71] S.A. Abouelmagd, B. Sun, A.C. Chang, Y.J. Ku, Y. Yeo, Release kinetics study of poorly water-soluble drugs from nanoparticles: are we doing it right? Mol. Pharm. 12 (2015) 997–1003, https://doi.org/10.1021/mp500817h.
[72] A. Bulle, K.H. Lim, Beyond just a tight fortress: contribution of stroma to epithelial-mesenchymal transition in pancreatic cancer, Signal Transduct. Targeted Ther. 5 (2020) 249, https://doi.org/10.1038/s41392-020-00341-1.
[73] B. Blanco-Fernandez, V.M. Gaspar, E. Engel, J.F. Mano, Proteinaceous hydrogels for bioengineering advanced 3D tumor models, Adv. Sci. 8 (2021) 1–38, https://doi.org/10.1002/advs.202003129.
[74] M.V. Monteiro, Y.S. Zhang, V.M. Gaspar, J.F. Mano, 3D-bioprinted cancer-on-a-chip: level-up organotypic in vitro models, Trends Biotechnol. 40 (2022) 432–447, https://doi.org/10.1016/j.tibtech.2021.08.007.
[75] L. Neufeld, E. Yeini, S. Pozzi, R. Satchi-Fainaro, 3D bioprinted cancer models: from basic biology to drug development, Nat. Rev. Cancer 22 (2022) 679–692, https://doi.org/10.1038/s41568-022-00514-w.
[76] G.G. Schwartz, et al., Pancreatic cancer cells express 25-hydroxyvitamin D-1α-hydroxylase and their proliferation is inhibited by the prohormone 25-hydroxyvitamin D3, Carcinogenesis 25 (2004) 1015–1026, https://doi.org/10.1093/carcin/bgh086.
[77] E. Glowka, J. Stasiak, J. Lulek, Drug delivery systems for vitamin D supplementation and therapy, Pharmaceutics 11 (2019) 347, https://doi.org/10.3390/pharmaceutics11070347.
[78] I. Sandez-Macho, M. Casas, E. V Lage, M.I. Rial-Hermida, A. Concheiro, C. Alvarez-Lorenzo, Interaction of poloxamine block copolymers with lipid membranes: role of copolymer structure and membrane cholesterol content, Colloids Surf. B Biointerfaces 133 (2015) 270–277, https://doi.org/10.1016/j.colsurfb.2015.06.019.
[79] N. Carragher, F. Piccinini, A. Tesei, O.J.T. Jr, M. Bickle, P. Horvath, Concerns, challenges and promises of high-content analysis of 3D cellular models, Nat. Rev. Drug Discov. 17 (2018) 606, https://doi.org/10.1038/nrd.2018.99.
[80] M. Rovithi, et al., Development of bioluminescent chick chorioallantoic membrane (CAM) models for primary pancreatic cancer cells: a platform for drug testing, Sci. Rep. 7 (2017) 44686, https://doi.org/10.1038/srep44686.
[81] Z. Zhao, et al., Intraductal papillary mucinous neoplasm of the pancreas rapidly xenografts in chicken eggs and predicts aggressiveness, Int. J. Cancer 142 (2018) 1440–1452, https://doi.org/10.1002/ijc.31160.
[82] K. Mitrevska, et al., Chick chorioallantoic membrane (CAM) assay for the evaluation of the antitumor and antimetastatic activity of platinum-based drugs in association with the impact on the amino acid metabolism, Mater. Today Bio 19 (2023) 100570, https://doi.org/10.1016/j.mtbio.2023.100570.
[83] J. Wang, et al., The role of micelle size in tumor accumulation, penetration, and treatment, ACS Nano 9 (2015) 7195–7206, https://doi.org/10.1021/acsnano.5b02017.

Further reading

[63] A. Abu-Fayyad, S. Nazzal, Synthesis, characterization, and in-vitro antitumor activity of the polyethylene glycol (350 and 1000) succinate derivatives of the tocopherol and tocotrienol isomers of Vitamin E, Int. J. Pharm. 519 (2017) 145–156, https://doi.org/10.1016/j.ijpharm.2017.01.020.
[65] D. Hwang, J.D. Ramsey, A.V. Kabanov, Polymeric micelles for the delivery of poorly soluble drugs: from nanoformulation to clinical approval, Adv. Drug Deliv. Rev. 156 (2020) 80–118, https://doi.org/10.1016/j.addr.2020.09.009.
[84] Y. Matsumoto, et al., Vascular bursts enhance permeability of tumour blood vessels and improve nanoparticle delivery, Nat. Nanotechnol. 11 (2016) 533–538, https://doi.org/10.1038/nnano.2015.342.